Western University
Scholarship@Western

Digitized Theses | Digitized Special Collections

1973

An Electron-microscopic Study Of Epitaxy, Magnetization And Domain Walls In Thin-films Of Permalloy

Anantaraman Ramakrishna Prasan

Follow this and additional works at: https://ir.lib.uwo.ca/digitizedtheses

Recommended Citation
Prasan, Anantaraman Ramakrishna, "An Electron-microscopic Study Of Epitaxy, Magnetization And Domain Walls In Thin-films Of Permalloy" (1973). *Digitized Theses*. 710.
https://ir.lib.uwo.ca/digitizedtheses/710

This Dissertation is brought to you for free and open access by the Digitized Special Collections at Scholarship@Western. It has been accepted for inclusion in Digitized Theses by an authorized administrator of Scholarship@Western. For more information, please contact tadam@uwo.ca, wlswadmin@uwo.ca.

CANADA

NATIONAL LIBRARY OF CANADA

CANADIAN THESES ON MICROFILM

BIBLIOTHÈQUE NATIONALE DU CANADA

THÈSES CANADIENNES SUR MICROFILM

16442

NL-101(1-66)

AN ELECTRON-MICROSCOPIC STUDY OF EPITAXY, MAGNETIZATION AND DOMAIN WALLS IN THIN FILMS OF PERMALLOY

by

Anantaraman Ramakrishna Prasan

Faculty of Engineering Science

Submitted in partial fulfillment
of the requirements for the degree of
Doctor of Philosophy

Faculty of Graduate Studies
The University of Western Ontario
London, Canada
June 1973

© Anantaraman Ramakrishna Prasan 1973

ABSTRACT

This thesis describes the measurement of domain wall width and magnetic polarization of well oriented epitaxial films of permalloy in (100), (110) and (111) orientation.

The films were deposited with simultaneous electron bombardment of the substrates under vacuum conditions of better than 10^{-8} torr on single crystal NaCl substrates of (100), (110) and (111) orientation. Film structure was determined by electron microscopy. The domain wall widths were determined by Lorentz electron microscopy using a technique due to Reimer and Kappert in which the widths measured at various defocussing distances are extrapolated to obtain the width at exact focus. For a determination of the magnetic polarization J_s, the electron microscope was used in the small angle diffraction mode in which a measurement of the deflection of the electrons in the film due to its spontaneous magnetic polarization directly gave the value of J_s with the help of a calibration carbon grating replica.

At a substrate temperature of 365 ^{o}C, the films evaporated with simultaneous electron bombardment were better oriented than those that were evaporated without

bombardment. The wall angles were less than π radian and their measured widths are comparable to those of Cohen and Harte (1969). The measured values of magnetic polarization were always less than bulk values which is also consistent with results published in the literature.

ACKNOWLEDGEMENTS

I am deeply indebted to my chief advisor Dr. J. D. Brown, Chairman, Materials Science Group for his guidance, advice, encouragement and constructive criticism. Dr. Brown supplied the much needed inputs at the right times in all the phases of this research without which this work would have been impossible.

I would also like to thank Dr. I. J. Duerden, Dr. G. A. Geach, Dr. C. Roy and Dr. J. S. Sheasby for their help and encouragement throughout the course of my studies at Western.

I would like to extend a special word of thanks to Dr. W. H. Wehlau of the Department of Astronomy for making the microphotometer facility available.

This research work was supported by funds from the National Research Council of Canada through Grants-in-Aid awarded to Dr. Brown and Faculty of Engineering, U. W. O.

TABLE OF CONTENTS

page

CERTIFICATE OF EXAMINATION ii

ABSTRACT iii

ACKNOWLEDGEMENTS v

TABLE OF CONTENTS vi

LIST OF TABLES ix

LIST OF FIGURES x

NOMENCLATURE xiii

CHAPTER 1 Introduction 1

CHAPTER 2 Epitaxial Films 12

2.1 Introduction 12

2.2 Variables Influencing Epitaxy 14

2.2.1 The Substrate 14

2.2.2 Temperature of the Substrate 15

2.2.3 Rate of Deposition 16

2.2.4 Film Thickness 17

2.2.5 Contamination 17

2.2.6 Electric Field 19

2.2.7 Electron Bombardment 19

2.2.8 X-Rays 19

2.3 Structural Defects in Epitaxial Films 20

2.4 Conclusions 21

CHAPTER 3 Reiview of Magnetic Domains and Lorentz Electron Microscopy 23

3.1 Introduction to Domains 23

3.2 Domain Walls 24

3.2.1 Bloch Wall 24

3.2.2 Néel Wall 25

3.2.3 Crosstie Wall 27

3.3 Domains in Single and Polycrystalline Films 27

3.4 Brown's Equations 28

3.5 Magnetic Polarization Distribution in a Domain Wall 32

3.6 Lorentz Microscopy 35

3.6.1 Introduction 35

3.6.2 Geometric Optic Theory 39

3.6.3 Validity of Geometric Optic Theory 46

3.6.4 Effect of Illumination Source Size 47

3.6.5 Effect of Small Angle Inelastic Scattering 49

3.7 Small Angle Electron Diffraction ... 50

CHAPTER 4 Experimental 52

4.1 Film Preparation 52

4.1.1 Source Material and Substrate 52

4.1.2 Evaporation System 52

4.1.3 Evaporation Procedure 56

4.2 Thickness Measurement 57

4.3 Electron Microscopy 58

4.3.1 Transmission and Diffraction Operation 58

4.3.2 Calibration of Image Magnification and Rotation . 61

4.3.3 Specimen Holder for Lorentz Microscopy 62

4.3.4 Determination of Illumination Aperture 66

4.3.5 Small Angle Electron Diffraction 67

4.3.6 General Experimental Procedure 72

4.4 Microphotometry 73

CHAPTER 5 Results and Discussion 75

5.1 Film Structure 75

5.2 Measurement of Magnetic Polarization 95

5.3 Measurement of Domain Wall Width ... 97

CHAPTER 6 Conclusions 108

APPENDIX 110

REFERENCES 113

VITA 120

LIST OF TABLES

TABLE — page

5.1 Summary of measured film thickness and magnetic polarization 95

5.2 Summary of measured wall widths 107

5.3 Wall widths in polycrystalline permalloy films measured by Cohen and Harte (1969) 107

LIST OF FIGURES

FIGURE		page
1.1	Magnetic storage capacity in 1968	4
3.1	Magnetization distribution in domain walls (a) and (b) Bloch walls; (c) and (d) Néel walls. (e) Crosstie wall	26
3.2	Spin distribution in a π rad Néel wall	34
3.3	(a) Trajectories of electrons passing through a magnetic film containing 2 π rad walls. (b) Intensity distribution in the image plane according to geometric and wave optics	38
3.4	Trajectories of electrons passing through a diverging domain wall and the resulting intensity distribution in the image plane	42
3.5	Intensity profiles for a converging and a diverging wall calculated according to geometric and wave optic theories	48
4.1	Film deposition system	55
4.2	Ray paths of (a) microscopy and (b) diffraction in the electron microscope	59
4.3	The special specimen holder for Lorentz microscopy	64

4.4 Calibration curve for the defocussing distance . 65

4.5 Ray diagram of the electron microscope when it is used as a small angle electron diffraction camera 68

4.6 (a) Small angle diffraction pattern from a 2160 lines/mm carbon grating replica (b) Splitting of a spot in the diffraction image due to Lorentz deflection of the electrons in the permalloy film 71

4.7 A typical photometer trace across a domain wall (z = 4.25 mm) 74

5.1 Transmission electron micrographs and diffraction patterns of permalloy evaporated onto cleaved (100) NaCl. (a) and (b) with no electron bombardment. (c) and (d) with simultaneous electron bombardment 77

5.2 Transmission electron micrographs and diffraction patterns of permalloy evaporated onto polished (100) NaCl. (a) and (b) with no electron bombardment. (c) and (d) with simultaneous electron bombardment 79

5.3 Transmission electron micrographs and diffraction patterns of permalloy evaporated onto polished (110) NaCl. (a) and (b) with no electron bombardment. (c) and (d) with simultaneous electron bombardment 81

5.4 Transmission electron micrographs and diffraction patterns of permalloy evaporated

onto polished (111) NaCl. (a) and (b) with no electron bombardment. (c) and (d) with simultaneous electron bombardment 83

5.5 Micrographs of a (111) film at different defocussing distances 101

5.6 (a) 2.374 rad wall in a permalloy film deposited on cleaved (100) NaCl. (b) 1.885 rad wall in a permalloy film deposited on polished (100) NaCl 103

5.7 (a) 2.217 rad wall in a permalloy film deposited on polished (110) NaCl. (b) 1.990 rad wall in a permalloy film deposited on polished (111) NaCl 105

A.1 Plot of the image half width as a function of defocussing distance for 1.990 rad wall in (111) film 111

NOMENCLATURE

A	exchange constant
$C(X,z)$	image contrast
d	diameter of the effective electron source; grating constant
e	electronic charge
$\hat{e}_j$	unit vector along j
$\hat{e}_s$	unit vector along $\vec{J}_s$
E	interaction energy
E_{an}	anisotropy energy
$\vec{F}$	Lorentz force
g	Landé g-factor
h	Planck's constant
$\hbar$	$= h/2\pi$
$\vec{H}_a$	applied magnetic field
$\vec{H}_d$	demagnetizing field
$I(\alpha)$	uniform intensity in the sample plane
$I(X,z)$	intensity in the image plane
$I(X_{1/2},z)$	intensity at half maximum
j	$= (-1)^{1/2}$
J_{ex}	exchange integral
$\vec{J}_s$, J_s	spontaneous magnetic polarization
J_x, J_y, J_z	x, y and z components of $\vec{J}_s$

K_1, K_2	anisotropy constants
l	nearest neighbor distance; distance from objective lens to selector aperture
L	effective camera length
m	mass of an electron
M_I, M_P	magnifications of intermediate and projector lenses
2r	split spot separation
$\vec{S}_i$, $\vec{S}_j$	spins of atoms i and j
$\vec{S}_v$	spin density
t	film thickness
$\vec{T}_a$	torque/unit volume due to applied field
$\vec{T}_{an}$	torque/unit volume due to anisotropy forces
$\vec{T}_{dm}$	torque/unit volume due to demagnetizing field
$\vec{T}_e$	exchange torque/unit volume
$\vec{T}_{tot}$	total torque/unit volume
v	volume/atom; velocity of electron
w_a	asymptotic wall width
$w_d(z)$	half width of domain wall as a function of defocussing distance z
$w_d(0)$	half width at exact focus (z = 0)
$2x_{1/2}$	$= w_d(0)$
$2X_{1/2}$	$= w_d(z)$
z	defocussing distance
z_o	distance of the effective electron source from the film

α	illumination aperture
α_1, α_2, α_3, α_j	direction cosines
α_s	inelastic scattering angle
γ	magnetomechanical ratio
δ	domain wall thickness parameter
θ	angle $\vec{J}_s$ makes with y-axis in a Néel wall
θ_{tot}	domain wall angle
λ	electron wavelength
μ_o	permeability of free space = $4\pi \times 10^{-7}$ henry/m
π	= 3.14159...
Σ	summation sign
ϕ	angle $\vec{J}_s$ makes with y-axis in Bloch wall; Lorentz deflection in a domain wall
ϕ_m	maximum Lorentz deflection
Φ	magnetic flux
τ	time
$L\lambda$	camera constant
∇^2	Laplacian operator

The author of this thesis has granted The University of Western Ontario a non-exclusive license to reproduce and distribute copies of this thesis to users of Western Libraries. Copyright remains with the author.

Electronic theses and dissertations available in The University of Western Ontario's institutional repository (Scholarship@Western) are solely for the purpose of private study and research. They may not be copied or reproduced, except as permitted by copyright laws, without written authority of the copyright owner. Any commercial use or publication is strictly prohibited.

The original copyright license attesting to these terms and signed by the author of this thesis may be found in the original print version of the thesis, held by Western Libraries.

The thesis approval page signed by the examining committee may also be found in the original print version of the thesis held in Western Libraries.

Please contact Western Libraries for further information:
E-mail: libadmin@uwo.ca
Telephone: (519) 661-2111 Ext. 84796
Web site: http://www.lib.uwo.ca/

CHAPTER 1

INTRODUCTION

G. W. Elmen showed in 1920 that alloys of nickel and iron containing 35 to 90% nickel have magnetic permeabilities much greater than that of iron. Such alloys are known as permalloys. In the composition range from 65 to 85% nickel the permalloy has unusual magnetic properties. Its magnetocrystalline anistropy is small and goes from positive to negative with zero anisotropy near the Ni_3Fe composition. At 81.5% Ni the magnetostriction is zero and as such it is called zero magnetostriction composition (ZMC). Because of the small anisotropy and magnetostriction, permalloys near ZMC are potentially suitable as magnetic memory elements.

The behavior of a magnetic material of finite dimensions is characteristic of its geometry. If one of its dimensions is made small ($\sim$100 nm) compared to that of the others ($\sim$10 mm) such as in the case of a thin film, then the sample exhibits two interesting properties. The first property is that a multidomain state is not energetically favorable. The magnetic polarization will be uniform and lies in the plane of the film. No domain wall

parallel to the plane of the film can exist in such a case. The second property is that for a uniformly magnetized film, the demagnetizing field due to the free poles at the edges is large within a few μm only. Therefore only very small reverse domains are found in a region constituting about 0.1% of the total volume. The film will thus be a single domain magnetized in a direction parallel to its plane. A permalloy film near ZMC has these properties and therefore produces a hysteresis loop that is nearly square in the easy direction and almost linear in the hard direction. It is thus suitable as a binary memory element.

The magnetic properties of permalloy in the thin film form have been extensively investigated in recent times (Chang and Feth 1964, Chang and Lin 1967) because of its potential application as a storage element in computers and other large electronic systems such as telephone networks and also because of its interesting magnetic state. Thin films for such applications can be manufactured by techniques similar to intergrated circuit manufacture and the two technologies are compatible. Their manufacturing process can easily be automated.

Since the time when Blois (1955) first reported the preparation of polycrystalline permalloy film, considerable though insufficient progress has been made in our understanding of its magnetic properties. But this hasn't prevented engineers from using them as storage elements due to an ever increasing need for faster and cheaper memories. Such

memories began appearing in commercial computers as early as 1966.

A thin film memory is made by evaporating permalloy on to glass in the presence of a magnetic field. It is usually deposited in the form of an array of rectangular spots each having a thickness of about 150 nm. The spots have cycle times of 100 to 500 nsec. A film memory does everything that a ferrite core does but is faster in speed and smaller in size. Its small size results in lower power dissipation and high speed in greater throughput than cores. The small size, high speed and low cost of film memories have made them very attractive to engineers. In its third generation computer B8500, Burroughs Corporation has included a 500 nsec main film memory of 16384 words of 52 bits each. There is a 200 nsec memory module of 2048 words of 64 bits each in the ILLIAC a giant parallel processor built by the same company for the University of Illinois. Figure 1.1 shows the magnetic memory capacity in use in 1968.

There is no doubt that in the future as our need for faster and more economical memories increases, the engineer will be called upon to fabricate magnetic materials for specific needs requiring careful matching and modification of the existing materials he now has to suit his new requirements. The materials engineers' goal of tailor making materials for such applications can only be realized if he has the necessary information on the film properties

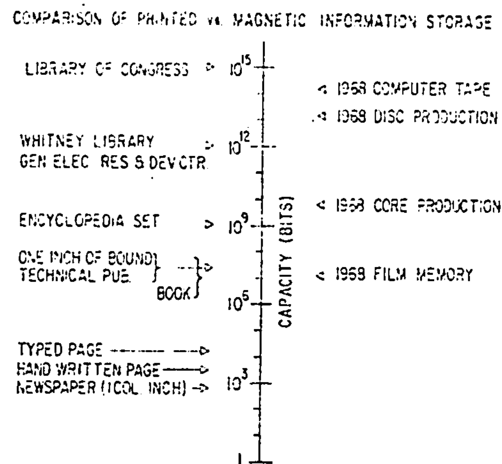

Figure 1.1 Magnetic storage capacity in 1968. [After Jacobs (1969)]

to predict and create the optimum in some desired combination of physical properties. Studies of ferromagnetic domains makes an important contribution to the understanding of magnetization process which is necessary for an effective use of thin films in such applications.

Domains and domain walls have been observed in thin films by the following techniques:

1. Kerr magneto-optic effect (Fowler and Fryer 1955).
2. Faraday magneto-optic effect (Williams et al. 1957 and Hale 1958).
3. Bitter technique (Williams and Sherwood 1957 and Huber et al. 1958).
4. Bitter replica technique (Craik and Griffiths 1958).
5. Lorentz electron microscopy (Hale et al. 1959).

The Kerr and Faraday techniques make use of the rotation of the plane of polarization of polarized light reflected from or transmitted through a magnetic film. There are experimental difficulties due to the small order of optical rotation produced which has thus limited their use. In the Bitter technique a fine colloidal suspension of magnetite is placed over the film. The 1 μm diameter colloid particles collect along the domain walls forming a pattern which is visible in a light microscope. Resolution of this technique is limited by the particle size. Craik and Griffiths (1958) have refined the Bitter technique by using 20 nm colloid particles suspended in sodium carboxy methyl cellulose. When the liquid film dries, it is peeled off the sample and it forms a replica for examination in the electron microscope. Even though this technique has improved resolution, it has the disadvantage that it produces static patterns only.

The increased resolution associated with transmission electron microscopy has led to the development of Lorentz electron microscopy which is reviewed in Chapter 3. With this technique domain structures can be studied in greater detail than has been possible hitherto. It has the added advantage in that the physical structure of the film can be examined at the same time as the magnetic structure. Resolution in this technique is about 1 to 5 nm which is about a hundred times better than the optical Bitter method and is able to give a wealth of detailed information. The electron microscope can also be used as a high resolution

small angle diffraction camera to measure spontaneous magnetic polarization J_s of ferromagnetic films. Its measurement by conventional methods such as a torque magnetometer requires equipments of high sensitivity.

A great proportion of research work reported in the literature has been on polycrystalline permalloy films. Although single crystal films of permalloy are of little practical use (Soohoo 1965), they greatly simplify the study of magnetic domains. Notwithstanding our limited understanding of the phenomenon of epitaxy, extensive use of it is being made in recent times as a means of producing crystallographically ordered films for study. The method consists of condensing the alloy from the vapor phase on to a suitable hot substrate in vacuum. Such substrates as NaCl, CaF_2, MgO, LiF and even epitaxial films of other metals have been used in the epitaxial deposition of permalloy films.

Epitaxial films of permalloy have been grown on NaCl by Heavens (1964), Boyd (1960), Burbank and Heidenreich (1960), Chikazumi (1961), Schoening and Baltz (1962), Lo (1966), Kirenskii et al. (1966a, b) and Alessandrini (1966) among others. Verderber and Kostyk (1961) have prepared epitaxial permalloy films on (100) and (111) faces of CaF_2, Tokutaka and Maejima (1965) on (110) LiF and Chikazumi (1961) on (100) MgO. Epitaxial permalloy films have also been grown successfully on epitaxial films of other metals grown on substrates of insulating materials.

For example, Collins and Heavens (1957), Heavens et al. (1961) and Heavens (1964) have grown films of Ni, Co, Fe and permalloy on epitaxial films of Cu which were in turn grown on NaCl and Pascard et al. (1972) have grown permalloy films in (111) orientation on epitaxial Au, Ag and Cu grown on mica.

Kirenskii et al. (1966a) employed 10^{-4} torr vacuum to grow epitaxial permalloy. They obtained films of varying crystal perfection on cleaved NaCl at substrate temperatures of 250 to 400 °C. Later they reported (Kirenskii et al. 1966b) obtaining approximately single crystal films at temperatures in the range of 160 to 200 °C. Boyd (1960) also worked in the same vacuum region but he deposited on cleaved NaCl at 526 °C. After annealing his films in the vacuum, he found a large density of stacking faults and twins (10^{15}-10^{17} m^{-2}). Heavens (1964) used slightly better vacuum (2×10^{-5} torr) and a lower substrate temperature (330 °C) than Baltz.

Burbank and Heidenreich (1960) and Schoening and Baltz (1962) deposited their films at residual gas pressures in the range of 10^{-5} to 10^{-6} torr. The former deposited 40 to 80 nm thick permalloy on (100) NaCl at 320 °C with the evaporation carried out for over 1 h. Their films were partially monocrystalline. The latter did similar experiments but obtained better results than Burbank and Heidenreich by annealing the partially monocrystalline films in the electron beam of the

microscope. It resulted in a more perfect film. Chikazumi (1961) obtained single crystal films on (100) NaCl which was preheated to 500 °C before they were cooled down to the deposition temperature. He does not specify the temperature of the substrate and the pressure in the evaporation chamber during evaporation. It is quite possible he used a 10^{-5} to 10^{-6} torr system. Since no examination of the films were made in the electron microscope by him, there is no way of knowing their quality. Lo (1966) and Alessandrini (1966) worked in 10^{-6} torr vacuum. Lo's films were obtained at 400 °C on (100) NaCl and were approximately single crystalline. Alessandrini on the other hand grew her films at 350 °C on (100) NaCl which had been preheated to 500 °C. She annealed the films in vacuum at 700 °C.

To compare the effect on epitaxy of different residual gas pressures during the evaporation, Baltz (1963) evaporated permalloy on (100) NaCl at 10^{-5} and 10^{-9} torr. After a 500 °C bakeout of the substrates, he deposited the films at 350 °C and found that ultra high vacuum improved epitaxy.

Epitaxial permalloy films of varying perfection have been obtained by the above workers at different pressures and substrate temperatures. The fact that vacuum conditions during film formation very strongly affect its structural perfection has been shown conclusively by the careful experiments of Baltz (1963). He found that

films evaporated at 10^{-5} torr were polycrystalline whereas those obtained at 10^{-9} torr were single crystalline which seems to contradict the results of others who grew their films at 10^{-5} to 10^{-6} torr. Such poor vacuum conditions in addition to producing films of poor quality, can incorporate structural defects in them. Alessandrini (1963) has shown that stacking faults appear by evaporating or annealing in vacuums of 10^{-5} torr and has attributed this effect to the presence of oxygen. In general films grown in moderate or high vacuum are less perfect and are badly contaminated compared to those of ultra-high vacuum (UHV). It is therefore necessary to deposit films in UHV for better results. There is also the added advantage in that the amount of gases trapped in the film is much smaller. Behrndt (1962) has shown that trapped gases do affect the coercivity of magnetic films.

Magnetic properties of permalloy films are known to depend on the substrate surface roughness. The surface of a substrate must be smooth in order to obtain films of reproducible characteristics. Sella and Trillat (1964) have shown that for NaCl substrates heated to over 500 °C thermal etching produces a surface covered by square pyramids visible even in an optical microscope. Therefore if NaCl is to be used as a substrate, thermal etching imposes a limit on the deposition temperature. But depositions at lower substrate temperatures do not produce good epitaxial orientation. Schoening's and Baltz's (1962)

method of evaporating permalloy on NaCl at moderate temperatures (320 °C) followed by annealing the films in the electron beam of the microscope is not very desirable in view of the poor vacuum conditions ($\sim 10^{-4}$ torr) prevailing in it. Any annealing must be carried out in a UHV system.

It has been known for some time that electron irradiation of substrates of insulating materials either before (Palmberg et al. 1967a) or during (Stirland 1966, 1967/68) the deposition influences the growth of epitaxial films. The irradiation lowers the temperature at which epitaxy is achieved. Stirland (1966) obtained single parallel orientation of gold at 10^{-6} torr on vacuum cleaved NaCl at 150 °C by bombarding the substrate with 90 eV electrons at a rate of 10^{17} electrons m^{-2} sec^{-1}. Kunz et al. (1966) also reported an improvement in epitaxy due to electron bombardment. Similar improvement was noticed by Palmberg et al. (1967a) who grew epitaxial Au and Ag on KCl with 40 eV electrons at rates of 10^{20} electrons m^{-2} sec^{-1}. Chambers and Prutton (1967a, b) used relatively high energy electrons ($\sim$7 kV) at rates of 5×10^{18} electrons m^{-2} sec^{-1} and pressures of 10^{-6} torr to obtain near perfect epitaxy of Ni on NaCl at 300 to 380 °C.

The purpose of the investigation reported in this thesis was to obtain good epitaxial films of permalloy in UHV on NaCl at moderate substrate temperatures and to measure the domain wall widths by Lorentz electron

microscopy and magnetization by small angle electron diffraction. The advantage of using NaCl substrate is that it is easily obtainable as a single crystal and the deposit is quickly stripped by water dissolution without contaminating it. Almost all the studies of films grown on NaCl so far have been on its (100) cleavage plane. Only two investigations have been reported in the literature in which growth has been achieved on (110) and (111) planes also. Collins and Heavens (1957) and Heavens et al. (1961) grew epitaxial films of Ni, Co, Fe and permalloy on the above three low index planes of NaCl at 10^{-5} torr. The other work is that of Grenga et al. (1971) who deposited epitaxial films of Ni on NaCl like Heavens et al. on the same three planes of NaCl except that they worked in better vacuum ($\sim 10^{-7}$ torr). Their paper was published when the present investigation was in progress. Heavens et al. worked in moderate vacuum but give little information on the quality of their permalloy films. It is interesting to note that while Heavens et al. deposited Ni films at 330 °C, Grenga et al. deposited their Ni films at 415 to 420 °C. Different experimental results are difficult to compare in the case of evaporated thin films as the evaporator is a dynamic system in which the experimental condition can vary very much. In general, evaporation in better vacuum produces films with more reproducible properties.

CHAPTER 2

EPITAXIAL FILMS

2.1 Introduction

In 1928 Royer introduced the term: epitaxy. It was derived from a greek word meaning "arrangement on".

Epitaxy is a special case of a more general phenomenon of the crystalline growth of a material on a substrate. It occurs when the substrate is a single crystal such that there exists a crystallographic relationship between the overgrowth and the substrate. There are two kinds of epitaxy namely, autoepitaxy and heteroepitaxy. The former refers to the growth of a single crystalline film on a substrate of the same material and the latter when the two are different. In the published literature it is common practice to use the two terms heteroepitaxy and epitaxy synonymously.

The phenomenon of epitaxy has been known for more than a century. It was first observed in minerals in which crystals of different chemical composition grew together with a definite crystallographic relationship between them. The earliest known attempt to achieve epitaxy in the laboratory seems to be that of M. L. Frankenheim who

in 1836 grew in parallel orientation sodium nitrate from solution on the surface of a calcite crystal.

A lot of work has been done in recent years to understand the nucleation and growth of thin films. Notable among them has been the work of Bassett (1960), Pashley and Stowell (1962), Pashley et al. (1964) and Poppa (1965). These authors grew evaporated films inside the electron microscope and were able to study the film growth directly. Their work indicates that in general there are four stages in the growth of an fcc metal film on a substrate of an insulating material. The first stage is called the nucleation stage in which a sudden burst of nuclei of the depositing material of uniform size (2 to 3 nm) is observed on the substrate surface as the evaporation begins. These nuclei grow in the second stage into three dimensional islands. The growth in the second stage takes place by the direct incorporation of impinging atoms from the source and capture of diffusing atoms on the substrate surface. When these islands grow big enough to touch one another, a very interesting phenomenon takes place. One island flows into another as two drops of a liquid will coalesce when in contact - the so-called "liquid-like" behavior. As the growth proceeds, the third stage called the channel stage is reached. In this stage the large coalesced islands join together to form a network structure with long, irregular and narrow channels separating the deposit material. The film has become electrically continuous at

this stage and contains holes and channels. In the final stage, the holes and channels are filled to form a continous film.

The mechanisms involved in the early stages of film growth are not well understood. It is believed that in the growth of epitaxial films the initial orientation of the nuclei is important, but the deciding factor is the recrystallization process that accompanies coalescence.

The various stages in the growth process of an epitaxial film can be significantly influenced by the deposition and the substrate variables. The rest of this chapter will briefly review those factors that are believed to be important in the light of present day knowledge and the final defect structure of epitaxial films.

2.2 Variables Influencing Epitaxy

The nature of the substrate and the various deposition parameters control the perfection of epitaxy. In this section a brief description of the different variables that must be optimized is given.

2.2.1 The Substrate

In the epitaxial growth of a thin film, the choice of the substrate is very important. A single crystal having a well defined low index plane exposed for the deposition of the film is always used.

On the basis of his experiments Royer gave a rule in 1928 which required a small misfit (less than 15%) for epitaxy to occur between the deposit and the substrate. In 1951 Schulz showed that this criterion is invalid by

growing epitaxial films on substrates involving misfits larger than 15%. More recently epitaxial films involving very large misfits have been grown. Two extreme examples are Sn/Ag: +101% and Ni/NaCl: -38%. Most present day investigators agree that a small misfit is important but not essential for epitaxy. In fact the key to a real understanding of epitaxial phenomenon is thought to be hidden in this.

The topography of the substrate could be important also. For example the cleavage steps on the surface of the substrate seem to aid nucleation. The degree of orientation of a continuous film grown on heavily stepped surfaces has been observed by many workers (Matthews 1966, Alpress and Sanders 1964) to be better than that grown on a smooth surface. On the other hand Heavens (1964) obtained better films of Ni and Ni-Fe on polished NaCl than on cleaved NaCl.

2.2.2 Temperature of the Substrate

Heating a substrate in vacuum has the following effects:

1. desorption of the absorbed contaminants,
2. lowering of supersaturation and thereby allowing adatoms sufficient time to reach equilibrium positions,
3. providing activation energy for adatoms to occupy positions of alignment with the substrate lattice and

4. increasing surface and volume diffusion between coalescing islands resulting in recrystallization.

If the rate of evaporation is held constant, then the nucleation rate varies inversely as the substrate temperature.

Until recently it was thought that there exists a critical temperature called an epitaxial temperature above which the epitaxy was perfect and imperfect below. However recent work has shown that for the same deposit-substrate combination the epitaxial temperature can vary over a wide range depending on the experimental conditions. For example, the epitaxial temperature of Au on NaCl depends on the prevailing vacuum conditions and whether the substrate was cleaved in air or vacuum just before the evaporation. In ordinary vacuum ($\sim 10^{-5}$ torr), the epitaxial temperature for Au on NaCl decreases if the crystal is cleaved in vacuum. On the other hand cleavage in ultra high vacuum produces poor epitaxy. Chopra (1969) even goes as far as to reject the whole concept of epitaxial temperature. Even though an epitaxial temperature does not exist for a deposit-substrate system, it does exist for the particular deposition conditions during the preparation of an epitaxial film.

2.2.3 Rate of Deposition

For a given substrate temperature epitaxy in general improves with a reduction in the rate of deposition.

Sometimes high rates of deposition promote epitaxy by increasing the temperature of the substrate and desorbing any substrate surface contamination. It also increases the nucleation rate; i.e., produces more stable nuclei by raising the supersaturation. Finally high rates reduce residual gas contamination in the film.

2.2.4 Film Thickness

In the initial stages of the film growth the three dimensional islands are practically free of structural defects. As growth proceeds, defects are incorporated into the film. It has been found that beyond a certain thickness poor orientation results.

In certain cases, an increase in film thickness improves epitaxy. Matthews (1965a, 1966) has found that during coalescence the initially misoriented nuclei reorient themselves. Such orientation changes occur by diffusion and grain boundary migration during the coalescence of two differently oriented nuclei.

2.2.5 Contamination

Contamination is always present in any vacuum system. Contamination cannot be eliminated completely even though it can be reduced in practice if proper care is taken. The sources of contamination are the residual gases, contamination from the substrate surface picked up during its preparation, gases from the source material and the heaters and gas desorption from the walls of the evaporator system. Interaction of the residual gases with the hot

source material and heater may also produce impurities. O_2, H_2O and CO_2 react with refractories with low carbon content and lead to the formation of oxides which are volatile at temperatures used for the evaporation of many metals. At the same time ions are also produced.

Contamination makes the adherence of the film to the substrate poor. It can also ruin or aid epitaxy depending on how it affects nucleation. Shinozaki and Sato (1965) found that a deliberate introduction of water vapor improves the epitaxy of Fe on NaCl. Green et al. (1970) have obtained good epitaxial films of Au on vacuum cleaved NaCl at room temperature by leaking chlorine into their UHV system.

For good epitaxy, one needs to remove those contaminants that have a detrimental effect and introduce those that have a beneficial effect. Matthews (1965a, 1966) found that air cleaved NaCl had twice as many nuclei generated per unit area as vacuum cleaved NaCl even though both came from the same parent crystal. The contaminants therefore increase the number of initial nuclei resulting in early coalescence during their growth.

The role of contaminants in nucleation and subsequent growth is very complex and as such is not clear at present. It can be said that impurities influence the nucleation process mainly by increasing the number of nuclei generated along with some minor changes in their orientation and probably changes in orientation of islands during

coalescence.

2.2.6 Electric Field

Chopra (1965) discovered that an application of a dc electric field in the plane of a substrate surface during the deposition induced coalescence of the nuclei at an early stage of film growth. The film became continuous at a lower average thickness than was normally observed. He found that a field of 10^4 V/m produced parallel orientation of Ag on freshly cleaved NaCl at 200 °C whereas a similar film produced without the application of electric field was polycrystalline.

2.2.7 Electron Bombardment

Electron bombardment of a substrate surface prior to film deposition affects epitaxy. Improvements in film orientation due to electron bombardment of alkali halide substrates has been known for some time (Bauer et al.1966, Green et al. 1962). It has been studied in detail by Stirland (1966) and Palmberg et al. (1967b).

Electron bombardment cleans the substrate surface by desorbing the absorbed gases and creates defects on the substrate surface. These defects increase the initial density of nuclei thereby leading to early coalescence. They may also affect the initial orientation of nuclei.

2.2.8 X-Rays

Inuzuka and Ueda (1968) reported improvement in epitaxy by irradiating NaCl with X-rays before deposition. The production of color centers in NaCl by CuKα radiation

resulted in three times as many nuclei as on an unirradiated sample. At a substrate temperature of 80 ^{o}C these color centers promoted parallel growth of films on the (100) cleavage plane of NaCl.

2.3. Structural Defects in Epitaxial Films

Structural defects are incorporated into films during their growth. The types of defects that are common in epitaxial films are:

1. stacking faults,
2. twins,
3. multiple positioning boundaries,
4. defects due to point defect aggregation (dislocation loops, stacking fault tetrahedra etc.) and
5. dislocations.

In fcc metal films stacking faults are present which extend from one surface of the film to the other. The stacking faults occur on all the {111} planes. They are also known to occur in a bent form extending from one {111} plane to another and have been seen intersecting one another on non parallel {111} planes. The fcc metal films also contain a high density of microtwins. The twinning occurs on all four {111} planes. Ino (1966) has observed even multiple twinning in Au grown on UHV cleaved NaCl. Multiple positioning boundaries are also very common. Its most common form is the double positioning boundary. If two (111) nuclei oriented such that they are related by a

π rad rotation join together during growth a double positioning boundary is formed. In fcc films double positioning is equivalent to twinning. Dislocation densities of thin films are also very high. Typically the density is in the range of 10^{14} lines/m^2 and the lines extend from one face of the film to the other through the shortest path. Usually the dislocations are absent in the initial nuclei but they begin to appear during the network stage of film growth. There is another kind of dislocation that appears in metal films if the misfit between the substrate and the deposit is less than 5%. They are the interfacial dislocations accommodating any misfit between the two lattices.

2.4 Conclusions

From the discussion of this chapter, it is quite obvious that the various experimental factors play a very complex role both independently and in combination in determining the final perfection of an epitaxial film. The roles of the substrate, its surface defect structure, contamination and other factors are not understood at present. Even the role of initial nucleation itself is not clear due to the limitations on resolution imposed by the present day electron microscopes and their poor vacuum. The nuclei that can be studied would have grown to atleast 2 nm in diameter which is much larger than the critical nucleus.

Our lack of sufficient understanding of the epitaxial

phenomenon perhaps explains why some times the work done at two different laboratories on the same deposit-substrate system seem to contradict one another. The ultra high vacuum evaporator is a dynamic system and it is very difficult to duplicate ones own work on a different day let alone someone else's. It is therefore not possible to predict the outcome given the prevailing experimental conditions. Obtaining a good epitaxial film is a matter of trial and error and the situation in this field is very similar to that in metallurgy before physics made its impact on it when the production of good steel was more an art than science.

Experimental studies of the surface of substrates and monolayer thick deposits are being done using LEED and Auger Electron spectroscopy. This information coupled with the possible future use of electron microscopes of the type developed by Professor Albert V. Crewe of the University of Chicago that can "see" atoms to study critical and subcritical nuclei should some day in the future unravel the mystery of epitaxial phenomenon.

CHAPTER 3

REVIEW OF MAGNETIC DOMAINS AND LORENTZ ELECTRON MICROSCOPY

3.1 Introduction to Domains

A ferromagnetic specimen can be magnetized to saturation by applied fields as small as 1 A/m. In order to explain this Pierre Weiss proposed in 1907 his now famous Molecular Field Theory which in addition to explaining the above mentioned phenomenon, predicted magnetization in such samples even at zero applied fields.

To reconcile the prediction of his theory with the experimentally observed demagnetized state of ferromagnetic specimens, Weiss postulated regions in the material spontaneously polarized with the direction of polarization different in different regions. Later experiments, especially those of Barkhausen and Bitter confirmed the existence of such domains.

According to the domain theory, each domain is saturated with its polarization vector $\vec{J}_s$ pointing along a specific direction. At a boundary separating the domains, the vector $\vec{J}_s$ does not change its direction abruptly. It always undergoes a transition from one direction in a domain to another in the next over a

finite distance. This transition region is called a domain wall. The domain concept explains the fact that although the exchange forces that are responsible for parallel alignment of the spins are equivalent to internal fields $\sim 10^9$ A/m, bulk magnetization can be radically altered by relatively small applied fields. The magnetization proceeds by the growth of more favorably oriented domains at the expense of those less favorably oriented by the movement of domain walls.

Even with all its successes, the domain theory is as Professor William F. Brown, Jr., states "a patch work of approximate concepts and formulas .... . It is far from complete in itself; it continually appeals to experiment for guidance" (Brown 1962).

3.2 Domain Walls

In ferromagnetic films, three types of domain walls are observed. They are the Bloch, Néel and intermediate walls. The intermediate walls are a superposition of a Bloch component and a Néel component.

3.2.1 Bloch Wall

Landau and Lifshitz proposed this model of a domain wall in 1935. Such walls are observed in bulk ferromagnetic samples and thick films. In a Bloch wall, the magnetic polarization vector rotates in the plane of the wall. Brown and Labonte (1965) have recently calculated the lower limit of film thickness for such walls to occur and find it to be about 70 nm based on $J_s = 1$ T and $K = 10^2$ J/m^3.

Figure 3.1(a) and (b) show a π radian Bloch wall. Here the component of magnetic polarization in the plane of the film and parallel to the wall normal is constant. The stray field therefore is normal to the plane of the film. If $\vec{J}_s$ makes an angle ϕ with the y-axis, its components in the wall are:

$$J_x = 0$$

$$J_y = J_s \cos \phi$$

$$J_z = J_s \sin \phi.$$

3.2.2 Néel Wall

It was shown by Néel that for thin films if the spin rotates in the plane of the film, the resulting wall will have a lower energy than a Bloch wall. Such a wall is called a Néel wall and occurs in thin films only. Because the polarization is in the plane of the film, the stray field is also in the plane of the film. Néel (1955) and Middelhoek (1963) suggested that such walls should be present in films less than about 20 to 50 nm thick. Middelhoek in his calculation assumed that the polarization rotates linearly across the wall and used the values 1 T and 10^2 J/m^3 for magnetic polarization and uniaxial anisotropy constant respectively.

From Figure 3.1(c) and (d) we see that if $\vec{J}_s$ makes an angle θ with the y-axis, its components are:

$$J_x = J_s \sin \theta, \; J_y = J_s \cos \theta \text{ and } J_z = 0.$$

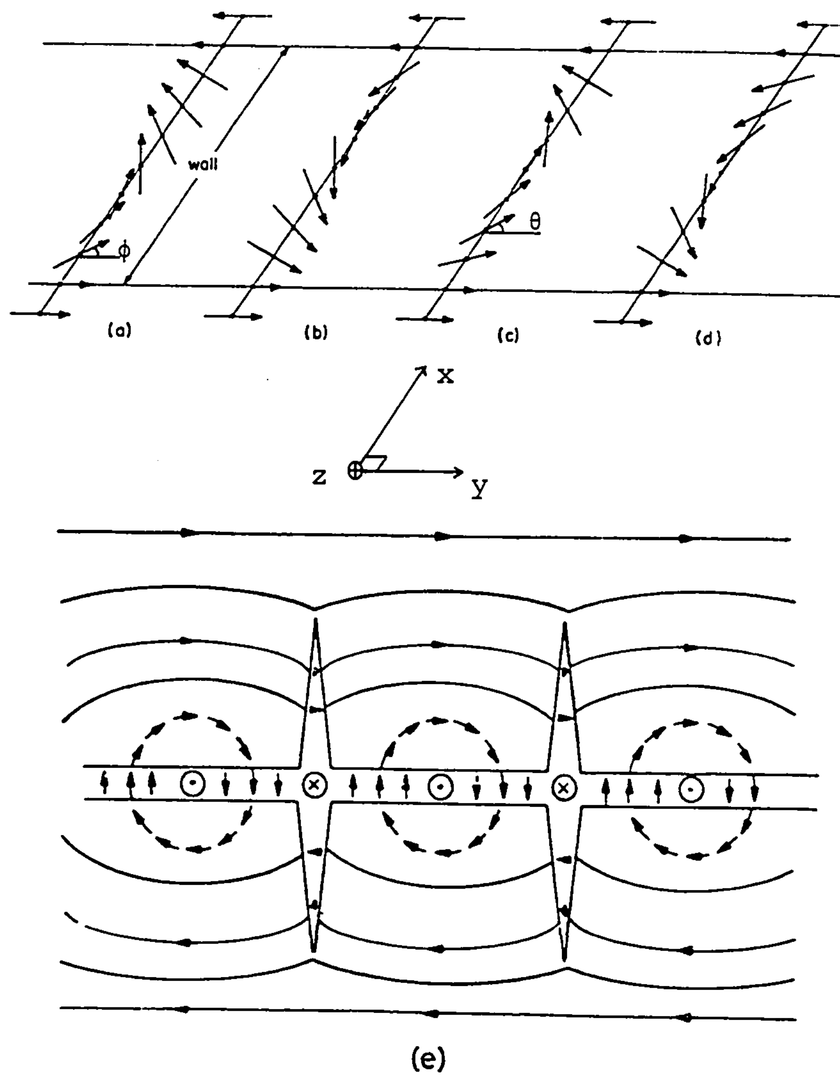

Figure 3.1 Magnetization distribution in domain walls.

(a) and (b) Bloch walls; (c) and (d) Néel walls. [After Middelhoek 1971.]

(e) Crosstie wall. [After Cohen 1969.]

3.2.3 Crosstie Wall

As film thickness increases, a Néel wall does not suddenly change to a Bloch wall at a certain critical thickness, but instead an intermediate wall structure called a crosstie wall results. It is a compromise between the Bloch and Néel modes of spin rotation. The stray field in this structure is neither in the plane of the film nor normal to it but somewhere in between. Huber et al. (1958) observed such walls in permalloy films.

From Figure 3.1(e) we see that the wall is interrupted by crossties at regular intervals. The length and period of crossties decrease with decreasing film thickness.

3.3 Domains in Single and Polycrystalline Films

Thin films are a few tens of nm thick and therefore the magnetic polarization is constrained to lie in the plane of the film. In other words thin films are said to have a shape anisotropy. In this sense the domain structure of thin films differs from that of bulk specimens where $\vec{J}_s$ need not be confined to any one plane.

In bulk polycrystalline materials, the grain size is usually larger than the domain size. Similarly in epitaxial films the grain size is larger than domain size so the domain structure while being modified by shape anisotropy is similar to that in bulk polycrystalline samples. In polycrystalline films on the other hand the grain size is much smaller than the domain size.

As a result their domain structure would be different from those of epitaxial films. It is mainly determined by magnetostatic considerations and not by the crystalline properties of individual grains.

3.4 Brown's Equations

For any quantitative analysis of the magnetization process one has to solve the so called Brown's equations which were first derived by W. F. Brown, Jr. (1940). In this section we shall briefly formulate his basic equations in three-dimensional form. To simplify matters we shall assume that the ferromagnetic specimen is mechanically rigid.

The sources of magnetic moment in a ferromagnetic material are the orbital motions and spins of electrons. Experiments indicate that the major contribution to ferromagnetism is from spins. Therefore one might safely say that ferromagnetism is due to the tendency of neighboring spins in a solid to align themselves parallel to each other.

It was Heisenberg who first suggested that ferromagnetism has its origin in the short range quantum mechanical exchange interaction. This interaction is of electrostatic origin and has no classical analog. The interaction energy of two spins $\vec{S}_i$ and $\vec{S}_j$ is given by

$$E = -2 J_{ex} \vec{S}_i \cdot \vec{S}_j \qquad (3.1)$$

where J_{ex} is called the exchange integral. If the exchange integral is positive, parallel alignment of spins results and if negative antiparallel alignment results. The exchange forces have a short range and act between the nearest neighbors only. Torques are produced whenever there is a slight change in the orientation of a spin from that of its neighbors.

It is reasonable to assume that any change in orientation of a spin from that of its neighbors in a solid is small compared to the lattice spacing. In other words the angle between the neighboring spins is small. In such a case we can treat the spins as classical vectors. The resultant exchange torque on the spin $\vec{S}_i$ is

$$2 \, J_{ex} \, \vec{S}_i \times \sum_j \vec{S}_j \tag{3.2}$$

where the sum is taken over the nearest neighbors of i. Since the angular variation of spins is assumed to be small, we can treat the variation of spin orientation as a continuous function of distance. The exchange torque per unit volume is then

$$\vec{T}_e = 2 \, J_{ex} \, l^2 \, v \, \vec{S}_v \times \nabla^2 \, \vec{S}_v \tag{3.3}$$

where $\vec{S}_v$ is the spin density, v is the volume per atom and l is the nearest neighbor distance. The local magnetic polarization $\vec{J}_s$ and the spin density are related by

$$\vec{J}_s = \gamma \, \hbar \, \vec{S}_v \tag{3.4}$$

where the constant γ is given by

$$\gamma = -\frac{g\,\mu_o\,e}{2\,m} \tag{3.5}$$

in which g is the Landé g-factor which is approximately equal to 2 and $\mu_o = 4\pi \times 10^{-7}$ H/m. $\hbar = h/2\pi$.
Therefore equation (3.3) becomes upon introducing equation (3.4) into it

$$\vec{T}_e = C\,\vec{J}_s \times \nabla^2\,\vec{J}_s \tag{3.6}$$

where

$$C = \frac{2\,J_{ex}\,l^2\,v}{\gamma^2\,\hbar^2}. \tag{3.7}$$

The effect of an applied field $\vec{H}_a$ on a magnetic material is to pull the magnetic polarization vector into its direction. The torque per unit volume due to the applied field is

$$\vec{T}_a = \vec{J}_s \times \vec{H}_a. \tag{3.8}$$

In a crystal, the magnetic domains are polarized along certain directions called the easy directions. A certain amount of work has to be done to rotate the polarization vector away from an easy direction. One can then say that the crystal exerts anisotropy forces to pull $\vec{J}_s$ into an easy direction. Such a coupling between the crystal lattice and the spin system can be represented by an anisotropy energy

$$E_{an} = E_{an}\ (\alpha_1,\ \alpha_2,\ \alpha_3) \tag{3.9}$$

where α's are the direction cosines of $\vec{J}_s$ relative to the reference directions in a crystal. For a cubic crystal the anisotropy energy is given by

$$E_{an} = K_1\ (\alpha_1{}^2.\alpha_2{}^2+\alpha_1{}^2.\alpha_3{}^2+\alpha_2{}^2.\alpha_3{}^2)\ +\ K_2\ (\alpha_1{}^2.\alpha_2{}^2.\alpha_3{}^2) \tag{3.10}$$

where α's are referred to the cube edges. K_1 and K_2 are anisotropy constants.

The torque per unit volume on $\vec{J}_s$ due to the anisotropy forces is

$$\vec{T}_{an} = -\ \hat{e}_s \times \sum_j \hat{e}_j \frac{\partial E_{an}}{\partial \alpha_j} \tag{3.11}$$

where $\hat{e}_s$ is a unit vector along $\vec{J}_s$ and $\hat{e}_j$'s are unit vectors along the easy directions of the crystal.

When a magnetic material of finite size is magnetized, magnetic poles are created at the surface. These poles give rise to a demagnetizing field $\vec{H}_d$ which exerts a torque on $\vec{J}_s$ to reduce the pole density. It is given by

$$\vec{T}_{dm} = \vec{J}_s \times \vec{H}_d. \tag{3.12}$$

The total torque per unit volume acting on the local magnetization is therefore

$$\vec{T}_{tot} = \vec{T}_a + \vec{T}_{dm} + \vec{T}_e + \vec{T}_{an} \tag{3.13}$$

and must be zero for equilibrium. Substituting equations (3.6), (3.8), (3.11) and (3.12), we obtain the equation

$$\vec{J}_s \times \left\{ (\vec{H}_a + \vec{H}_d) + C\,\nabla^2 \vec{J}_s - \frac{1}{|\vec{J}_s|} \sum_j \hat{e}_j \frac{\partial E_{an}}{\partial \alpha_j} \right\} = 0. \tag{3.14}$$

Equation (3.14) is a set of two nonlinear partial differential equations. The independent variables are the two direction cosines that describe the orientation of $\vec{J}_s$. According to Brown, they must be solved along with the boundary condition at a point on the surface

$$\vec{J}_s \times \frac{\partial \vec{J}_s}{\partial n} = 0 \tag{3.15}$$

where $\partial/\partial n$ is the differentiation along the outward normal to the surface of the specimen. Equations (3.14) and (3.15) are called Brown's equations. They are very difficult to solve and approximate solutions have been obtained for a few simple cases only. In the case of problems of engineering interest attempts to solve the above equations rigorously have proven to be fruitless.

3.5 Magnetic Polarization Distribution in a Domain Wall

In order to obtain an expression for the distribution of $\vec{J}_s$ across a domain wall in a finite crystal, Brown's equations (3.14) and (3.15) must be solved. Because of their nonlinear character the mathematics involved is

complex and as yet no one has been sucessful in obtaining exact solutions for real life problems. However, there has been several attempts at obtaining approximate solutions. Since the validity of all of them is debatable, the simplest and the most popular model due to Kittel (1949) will be described. As this model has been used by many workers, wall widths of this investigation can be compared with published data.

Let us consider an infinite uniaxial film in the x-y plane containing two domains separated by a Néel wall. $\vec{J}_s$ is assumed to be directed along +y at $x = -\infty$ and -y at $x = +\infty$. In this case the torques arise from exchange and anisotropy forces. The former tries as far as possible to reduce the rate of rotation of $\vec{J}_s$ by spreading out the width of the boundary while the latter opposes the rotation of $\vec{J}_s$ from the easy direction. The final wall configuration would be the one that balances these two forces. The solution of Brown's equation gives for the orientation of $\vec{J}_s$ as a function of x

$$x = \delta \ln \tan \left(\frac{\theta}{2}\right) \tag{3.16}$$

where θ is the angle between $\vec{J}_s$ and y-axis and the wall thickness parameter δ is given by

$$\delta = \left[\frac{A}{K_1}\right]^{\frac{1}{2}}. \tag{3.17}$$

A is the exchange constant. For fcc crystals it is equal

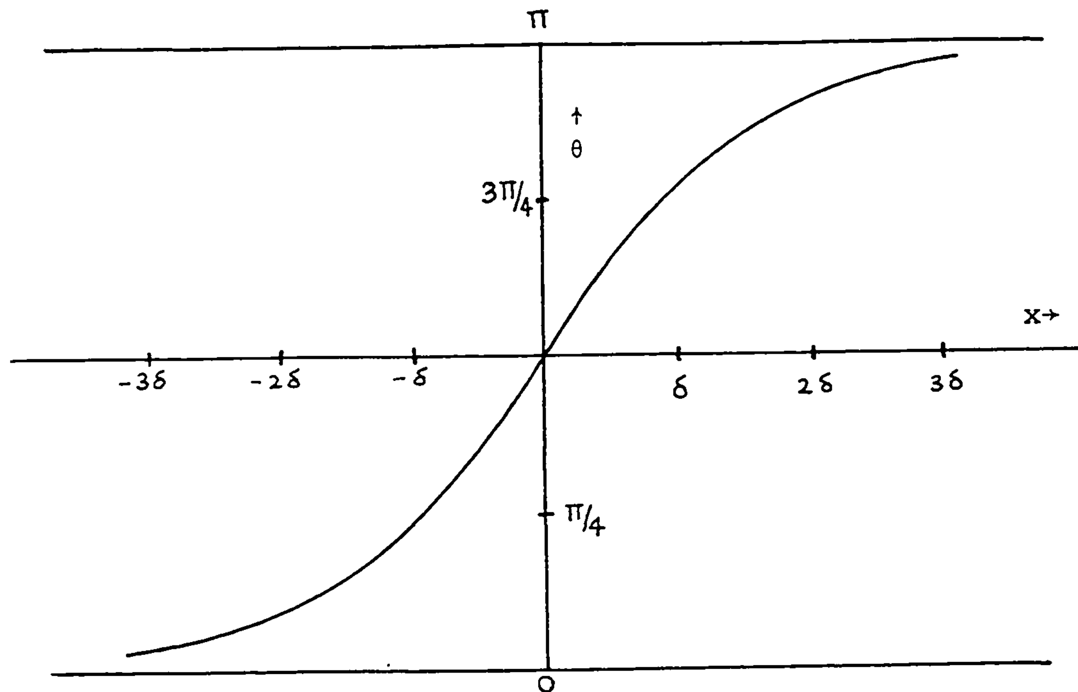

Figure 3.2 Spin distribution in a π rad Neel wall.

to ($4 J_{ex} S^2/a$) where a is the lattice parameter and S is the spin (it is assumed that the spins at all the lattice sites are equal; i.e., $|\vec{S}_i| = |\vec{S}_j| = S$).

Recasting equation (3.16) into another form we have

$$\theta = - \text{arc cot} \{\sinh (\frac{x}{\delta})\}. \qquad (3.18)$$

From equation (3.18) it is apparent that $\vec{J}_s$ rotates smoothly across the domain wall. In Figure 3.2, θ is plotted as a function of x. The wall width is infinite according to this model. We therefore define an asymptotic width w_a:

$$w_a = \frac{\theta_{tot}}{\left[\frac{d\theta(x)}{dx}\right]_{x=o}} = \theta_{tot} \cdot \delta \qquad (3.19)$$

where θ_{tot} is the wall angle. Within the range $-\delta \leqq x \leqq \delta$, 60% of the angular variation of $\vec{J}_s$ takes place. For a π rad wall, the asymptotic width is $\pi\delta$.

3.6 Lorentz Microscopy

3.6.1 Introduction

Hale et al. (1959), Fuller and Hale (1960a, b), Boersch and Raith (1959) and Boersch et al. (1960) showed that ferromagnetic domains can be studied by the techniques of transmission electron microscopy. This technique is called Lorentz microscopy as the magnetic structure is imaged in the microscope by the electrons deflected by the

Lorentz force in the specimen. The image contrast is obtained by defocussing the objective lens.

Many workers have subsequently used this technique to measure domain wall widths. They are Boersch et al. (1961b, 1962), Warrington (1964), Wade (1962), Suzuki et al. (1968), Ray and Paul (1970) and Hemenger (1964) to name a few. In most previous measurements of domain wall widths, the experimentally measured intensity determined from the photographic plate were compared with a calculated intensity profile. The intensity profile is calculated from an assumed spin destribution in the wall. Some workers instead of bothering to compute the whole intensity profile have just computed the values at distinct points such as the midpoint of a divergent wall and then compared it with measured values from photographic plates.

Again, most of the earlier workers have not taken into consideration the importance of illumination aperture of the electron source and the small angle scattering in the film on the domain wall image. Reimer and Kappert (1969a, b) have shown that these effects modify the image intensity especially in the middle of the wall. They show that the half width of the divergent wall image should be used as a measure of the domain wall width as it varies very little with change in illumination aperture.

The electron intensity distribution on the image plane can be calculated by either the wave optic theory or its limiting case, the geometric optic theory. Boersch

et al. (1961b, 1962) developed the wave optic theory in which they calculate the Kirchhoff diffraction integral. The amplitude at a point in the image plane is given by

$$U(X) = Ae^{jk[(z+z_0) + X^2/2z]} \times \int_{-\infty}^{+\infty} \exp j \left[- \frac{et}{\hbar} \int_0^x B_y(x)\, dx + k \left\{ \left(\frac{1}{z_0} + \frac{1}{z}\right)\frac{x^2}{2} - \frac{Xx}{z} \right\} \right] dx \tag{3.20}$$

where

$B_y(x)$ is the y component of saturation induction,

X is the coordinate in the image plane,

x is the coordinate in the sample plane,

z_0 is the distance of the virtual electron source from the sample,

A is a constant,

z is the defocussing distance and

k is the wave number of the electrons.

A calculation based on the wave optic theory is very cumbersome. On the other hand the geometric optic theory of Fuller and Hale is much simpler and will be described in the next subsection.

The theoretical intensity profiles of a convergent wall and a divergent wall according to wave optic and geometric optic theories calculated by Reimer and Kappert are shown schematically in Figure 3.3(b). It is clear that

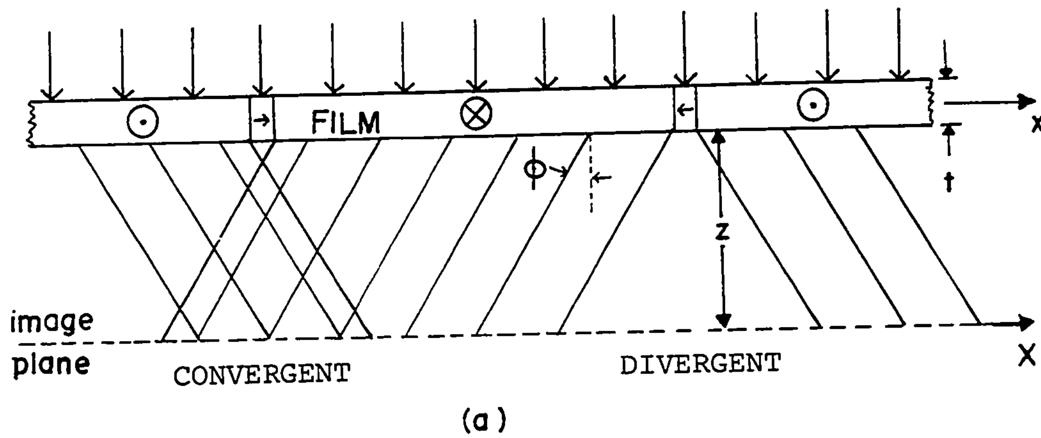

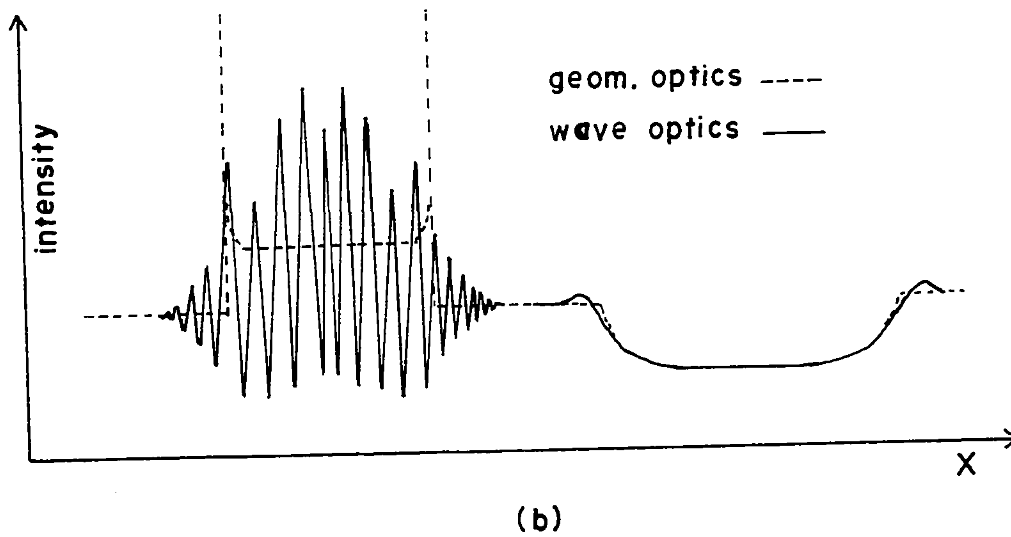

Figure 3.3 (a) Trajectories of electrons passing through a magnetic film containing 2 π rad walls.

(b) Intensity distribution in the image plane according to geometric and wave optics.

the difference between the two theories is significant only in the case of a convergent wall. The experimentally observed interference fringes in its image are correctly predicted by the wave optic theory. On the other hand the difference between the two theories in the case of a divergent wall is very small. The geometric optic theory can therefore be used only with divergent wall images. It must be mentioned that although Lorentz microscopy has been found to be very useful in the study of domain walls, no way has been found to determine the wall type.

3.6.2 Geometric Optic Theory

Figure 3.3(a) shows a magnetic film of thickness t and containing two π radian walls. The film lies in the x-y plane and is normal to the optic axis of the microscope which is along the z axis pointing downwards. The domain walls are parallel to the y-axis which is directed out of the paper.

The Lorentz force experienced by an electron travelling with a velocity v and incident on a magnetic film is given by

$$\vec{F} = -e\,\vec{v} \times \vec{J}_s \tag{3.21}$$

where -e is the electronic charge and $\vec{J}_s$ is the saturation polarization in the film. If $\vec{v}$ is along the z-axis and $\vec{J}_s$ is along the y-axis then the force experienced by the electron is directed perpendicular to the optic axis.

It is

$$m \frac{d^2x}{d\tau^2} = - evJ_s . \tag{3.22}$$

If this force only acts within the thickness t of the film, then

$$\frac{dx}{d\tau} = - \frac{e}{m} J_s \int_0^t v \, d\tau$$

$$= - \frac{etJ_s}{m} . \tag{3.23}$$

The maximum Lorentz deflection ϕ_m is given by

$$\phi_m = \frac{dx}{d\tau} \frac{1}{v}$$

$$= - \frac{etJ_s}{mv} . \tag{3.24}$$

For 100 kV electrons, equation (3.24) gives for ϕ_m a value around 10^{-5} radians. This deflection is much smaller than the aperture of the objective lens which is about 10^{-2} radian. As a result the magnetic structure in the image will vanish when the objective lens is focussed on the specimen. In order to image the domain wall, the film must be out of focus. In other words the object plane of the objective lens is not the plane of the specimen but a plane a few mm above or below the specimen in this mode of operation.

When a sample containing many domains is viewed in the electron microscope in the defocussed mode, some domain walls appear bright and some others dark. In Figure 3.3(a) we see that the electron beam coverges at the domain wall on the left hand side, whereas it diverges at the wall on the right hand side. If the image plane is below the film, the left wall would be bright and the right dark. The contrast is reversed if the image plane is above the film.

The width of the wall image at the object plane and hence the width on the photographic plate is proportional to

$$\begin{aligned} &2 z \phi_m + w \quad \text{for a diverging wall} \\ &2 z \phi_m - w \quad \text{for a converging wall} \end{aligned} \tag{3.25}$$

where z is the defocussing distance [see Figure 3.3(a)] and w is the wall width.

Inside the Néel domain wall, the y component J_y of the magnetic polarization $\vec{J}_s$ is a function of x because $\vec{J}_s$ rotates in the plane of the film between the domains. Therefore

$$J_y = \pm |\vec{J}_s| \qquad \text{inside a domain}$$

and

$$J_y = J_y(x) \qquad \text{inside a wall}$$

and the Lorentz deflection ϕ will be a function of x inside

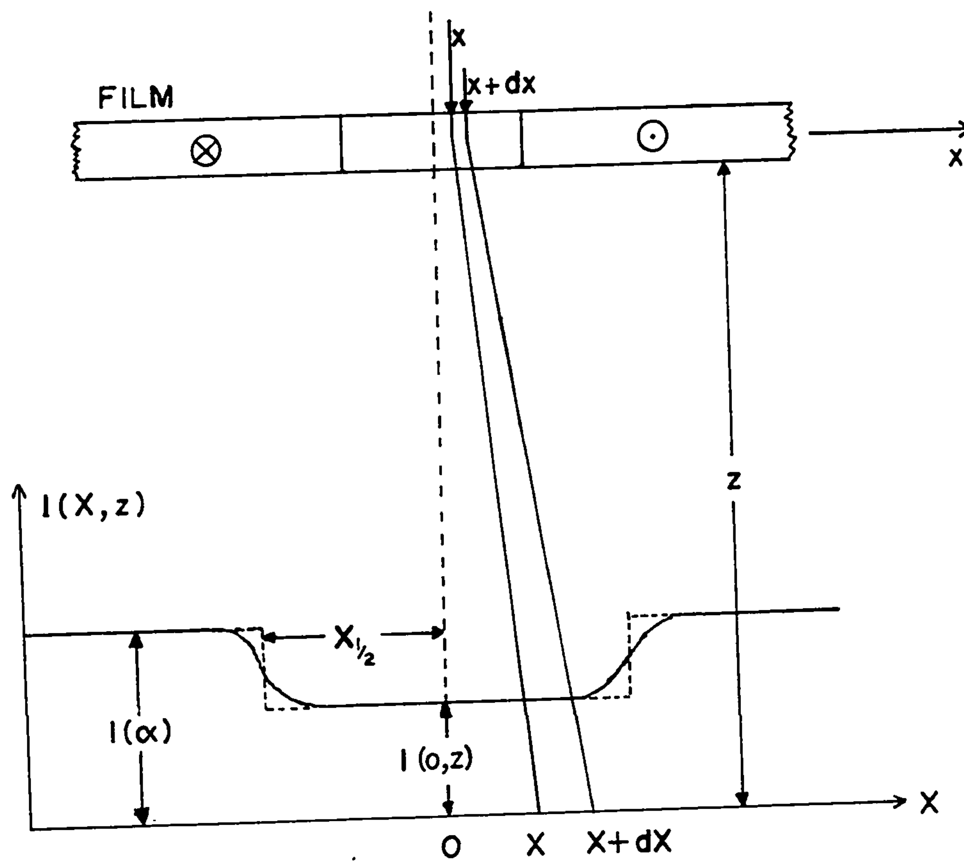

Figure 3.4 Trajectories of electrons passing through a diverging domain wall and the resulting intensity distribution in the image plane.

a wall. Figure 3.4 shows a diverging wall in the plane of a film. The middle of the wall is taken as the origin of the coordinate system. Then the Lorentz deflection in the wall is given by

$$\phi(x) = -\frac{etJ_y(x)}{mv} . \qquad (3.26)$$

Taking the ratio of this and the maximum Lorentz deflection occuring in a domain given by equation 3.24 we have

$$\frac{\phi(x)}{\phi_m} = \frac{J_y(x)}{J_s} . \qquad (3.27)$$

The image plane in Figure 3.4 is in the X-Y plane at a distance z below the x-y plane in which the sample lies. Therefore a point x in the domain wall is mapped into a point X in the image plane according to

$$X = x + z\,\phi(x)$$

$$= x + z\,\phi_m \frac{J_y(x)}{J_s} \qquad (3.28)$$

and

$$\frac{dX}{dx} = 1 + \frac{z\phi_m}{J_s}\frac{dJ_y(x)}{dx} \qquad (3.29)$$

If $I(\alpha)$ is the uniform intensity in the sample plane

and I(X,z) the intensity in the image plane, conservation of electrons requires that

$$I(\alpha)\ dx = I(X,z)\ dX$$

or

$$\frac{I(X,z)}{I(\alpha)} = \frac{dx}{dX} \tag{3.30}$$

Introducing equation (3.29) into equation (3.30) we have

$$\frac{I(X,z)}{I(\alpha)} = \left\{ 1 + \frac{z\phi_m}{J_s} \frac{dJ_y(x)}{dx} \right\}^{-1} . \tag{3.31}$$

The image contrast is defined by

$$C(X,z) \triangleq \frac{I(\alpha)}{I(X,z)} - 1$$

$$= \frac{z\phi_m}{J_s} \frac{dJ_y(x)}{dx} \tag{3.32}$$

From equation (3.32) we see that the contrast is maximum at the wall center where the gradient of $J_y(x)$ is maximum. Also at exact focus; i.e., z=0 there is no contrast.

In the lower part of Figure 3.4 the electron intensity is plotted as a function of distance X in the image plane. If $2X_{½}$ is the half width of the divergent wall image which corresponds to $2x_{½}$ in the wall, then the

intensity at half maximum is given by

$$I(X_{\frac{1}{2}},z) = \frac{I(\alpha) + I(0,z)}{2} \tag{3.33}$$

where I(0,z) is the intensity in the middle of the divergent wall. Using the above relation it can be shown that the gradients of the polarization component $J_y(x)$ evaluated at $x_{\frac{1}{2}}$ and x=0 are related through the following equation:

$$\left\{\frac{dJ_y(x)}{dx}\right\}_{x_{\frac{1}{2}}} = \frac{\left[\frac{dJ_y(x)}{dx}\right]_{x=0}}{2 + \frac{z\phi_m}{J_s}\left\{\frac{dJ_y(x)}{dx}\right\}_{x=0}} \tag{3.34}$$

when z=0, equation (3.34) says that the gradient of $J_y(x)$ at $x_{\frac{1}{2}}$ is half of that at the center of the wall.

The measured half width w_d of a wall at a defocussing distance z is according to equation (3.25)

$$w_d(z) = 2\, z\, \phi(x_{\frac{1}{2}}) + 2\, x_{\frac{1}{2}} \; . \tag{3.35}$$

To obtain the half width at zero defocussing distance; i.e., $w_d(0)$, one takes a series of defocussed pictures at different z and plots the measured half widths $w_d(z)$ as a function of z. A linear extrapolation to the ordinate

gives directly the half width $w_d(0)$. Reimer and Kappert have shown this to be true for a finite illumination aperture α provided $\alpha \leqq \phi_m$.

3.6.3 Validity of Geometric Optic Theory

Aharonov and Bohm showed in 1959 that Lorentz deflection of electrons in a magnetic film is a quantum phenomenon. Any explanation of the contrast formation would therefore require the full use of the wave optic theory of Boersch et al. (1961a, b, 1962). Wohlleben (1966, 1967) however showed that geometric optic theory is a limiting case of wave optic theory and the former theory is valid provided two criteria are satisfied.

The first criterion is that it is not possible to resolve classically the change in magnetic field between two points unless the flux enclosed by the two points is large compared to a fluxon. Therefore to resolve two points the difference in magnetic flux $\Delta\Phi$ between them

$$\Delta\Phi > \frac{h}{2e} \cdot \qquad (3.36)$$

Thus the sharpest detail in any Lorentz micrograph that can be observed involves a flux increment of at least 2.07×10^{-15} Wb. As far as this criterion is concerned, the validity of the classical theory varies as the thickness of the film.

The second criterion is that if the increment of magnetic flux is not large compared to a fluxon, then the

geometric optic result is similar to the wave optic result provided the defocussing distance z is small compared to the reciprocal of the gradient of Lorentz deflection $d\phi/dx$. For a 30 nm thick Ni-Fe film it would be approximately 5 mm.

3.6.4 Effect of Illumination Source Size

The electron beam used in the imaging of domain walls is seldom parallel as the source in practice always has a finite width. After emerging from the filament, the electrons suffer a crossover of finite diameter in the gun assembly. The condenser 1 lens produces a reduced image of the crossover which is then imaged slightly above or below the specimen by the condenser 2 lens. This second image forms the effective source and has a diameter d. If z_o is the distance of the effective source from the specimen, then the angle subtended at the specimen plane α is $d/2z_o$. By varying the excitation on the condenser lens, the illumination aperture α can be varied.

Reimer and Kappert (1969a) have studied the effect of the finite illumination aperture on the wall images. They find that as α increases, the fine structure in the images is lost. It has been found that the convergent wall images are more sensitive to the illumination aperture than divergent wall images and as α increases to 10^{-5} radian the fringes disappear in the convergent wall images completely.

Figure 3.5 shows schematically the intensity

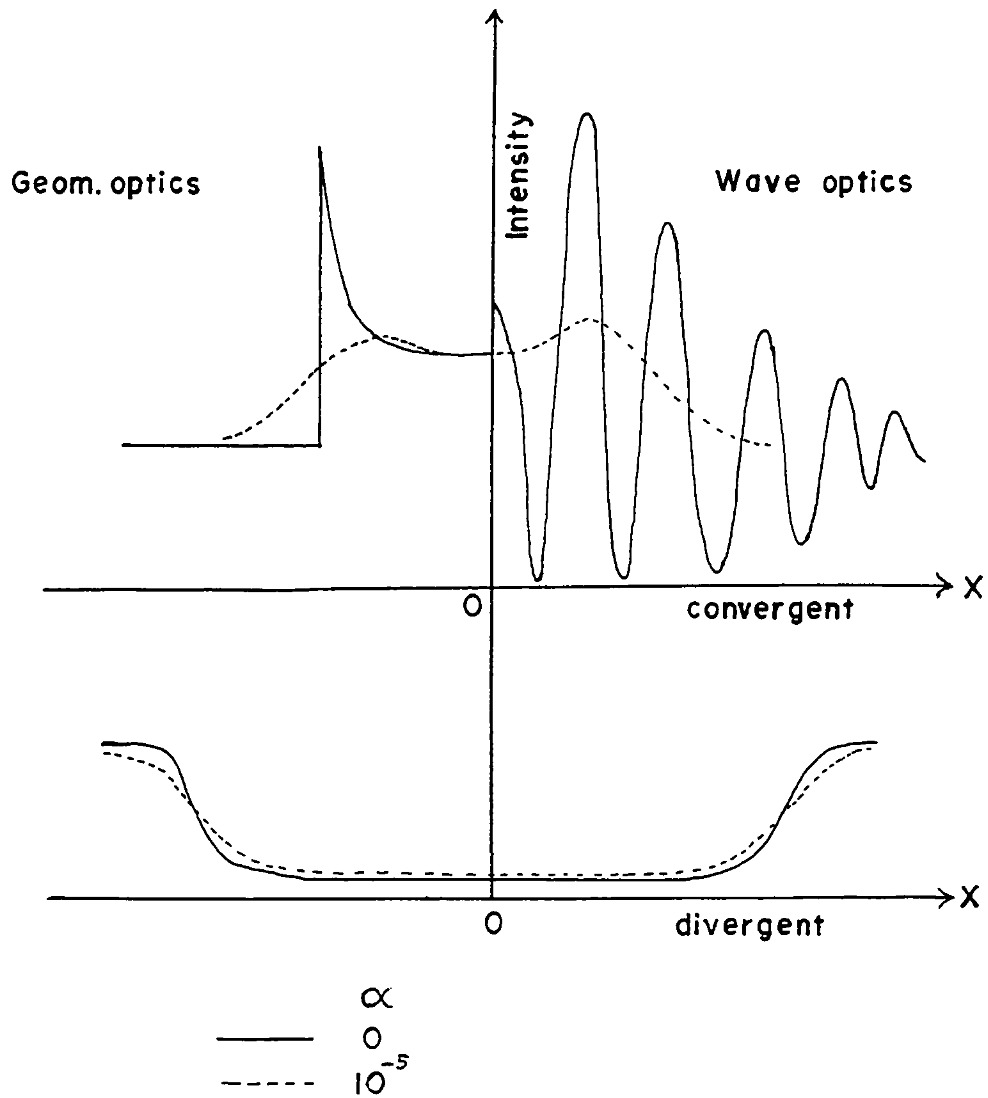

Figure 3.5 Intensity profiles for a converging and a diverging wall calculated according to geometric and wave optic theories.

distributions of a convergent and a divergent wall for $\alpha=0$ and 10^{-5} calculated according to both wave optics and geometric optics by Reimer and Kappert. It is apparent that the diverging wall image is insensitive (to a large extent) to variations of α. The other noticeable feature is that the half width has not changed at all even though the intensity in the middle of the divergent wall has slightly decreased. Therefore a measurement of wall thickness from the half width of a divergent wall image will give a result that is almost independent of the illumination aperture.

3.6.5 Effect of Small Angle Inelastic Scattering

Small angle inelastic scattering of electrons by the sample influences the contrast in domain wall images. The resulting beam broadening increases for films thicker than about 50 nm and at low accelerating voltages. The contrast at low voltages is essentially determined by the ratio of the Lorentz deflection ϕ and the inelastic scattering angle α_s.

The influence of small angle inelastic scattering on wall images was not taken into account by Suzuki et al. (1968) and Suzuki and Wilts (1969) in their work. They used the decrease in intensity in the middle of a divergent wall as a function of defocussing distance for wall width calculations. Their results were unreasonably large (about three times).

Reimer and Kappert (1969b) have considered this problem both for convergent and divergent walls. Their results show that for convergent walls, the inelastic scattering effect must be accurately known as it strongly influences the intensity distribution. On the other hand for divergent wall images, the scattering has negligible influence on the half width even though the total intensity curve is strongly modified. It is therefore possible to ignore the inelastic scattering effect and yet obtain reasonably accurate results if half widths of divergent wall images are used as a measure of wall width.

3.7 Small Angle Electron Diffraction

An electron microscope was used as a small angle diffraction camera for the first time by Mahl and Weitsch (1960). It was then used by Ferrier and Wade (1964), Ferrier (1964) and Mader and Nowick (1968) to measure the saturation magnetic polarization of thin films.

The maximum Lorentz deflection ϕ_m suffered by an electron passing through a ferromagnetic film is from equation (3.24)

$$\phi_m = - \frac{etJ_s}{mv}. \tag{3.24}$$

If the area illuminated by the electrons contains a π radian wall, then the incident beam is split during its passage through the film producing two spots separated

by a distance 2r on the photographic plate. The spot separation and Lorentz deflection are related through

$$\phi_m = \frac{r}{L} \tag{3.37}$$

where L is the effective camera length. We have from equations (3.14) and (3.37)

$$J_s = - \frac{mvr}{etL}. \tag{3.38}$$

By making use of the de Broglie relation, equation (3.38) can be rewritten as

$$J_s = - \frac{hr}{et(L\lambda)}. \tag{3.39}$$

The quantity $(L\lambda)$ is the camera constant and can be determined independently. If the thickness of the film is known, then J_s can be calculated.

CHAPTER 4

EXPERIMENTAL

4.1 Film Preparation

4.1.1 Source Material and Substrate

The 84.5 wt.% Ni and 15.5 wt.% Fe permalloy wire used for evaporation was supplied by the Precision Metals Division of Hamilton Watch Company. It is well known that in the evaporation of permalloy, the nickel content in the film is less than that in the source material with the result that the composition used in this study is expected to produce a film near the zero magnetostriction composition which is 81.5% Ni (Chopra 1969).

The substrates used were (100), (110) and (111) NaCl crystals supplied in the precut form by the Harshaw Chemical Company.

4.1.2 Evaporation System

The evaporation was carried out in a Vacuum Generators ultra high vacuum system which could be pumped down to 10^{-9} torr. A 50 liter/sec ion pump backed by two sorption pumps and a three element titanium sublimation pump pumped the system. The titanium sublimation pump was housed in the stainless steel vacuum vessel. A 0.3 m.

diameter and 0.35 m tall pyrex bell jar served as the evaporation chamber the seal for which was provided by a viton L gasket. The pressure was measured by the current drawn by the ion pump which was connected to the stainless steel chamber directly below the bell jar.

Both nickel and iron alloy readily with the tungsten filament during evaporation leading to its rapid disintigration. This can be prevented by ensuring that the permalloy makes up only one-third of the mass at any point along the filament (Chopra 1969). The evaporation source was constructed in the form of a double strand spiral to increase its surface area for wetting and the permalloy wire was wound around it so as to cause a uniform distribution of the melt over the whole spiral.

The substrates were heated by a OFHC copper block which was in turn heated by a tungsten filament. A tantalum heat shield was constructed around the filament. The temperature of the substrates could be measured by a Chromel-Alumel thermocouple embedded in a monitor NaCl crystal sitting with the substrates.

The evaporation source and the substrates were separated by 150 mm. Figure 4.1 illustrates the evaporation geometry. A shutter which could be operated magnetically from the outside was used to interrupt the evaporation.

A simple electron gun was designed to bombard the substrates with electrons before and/or during the evaporation.

(a)

(b)

Figure 4.1 Film deposition system. (a) Electron gun and (b) substrates.

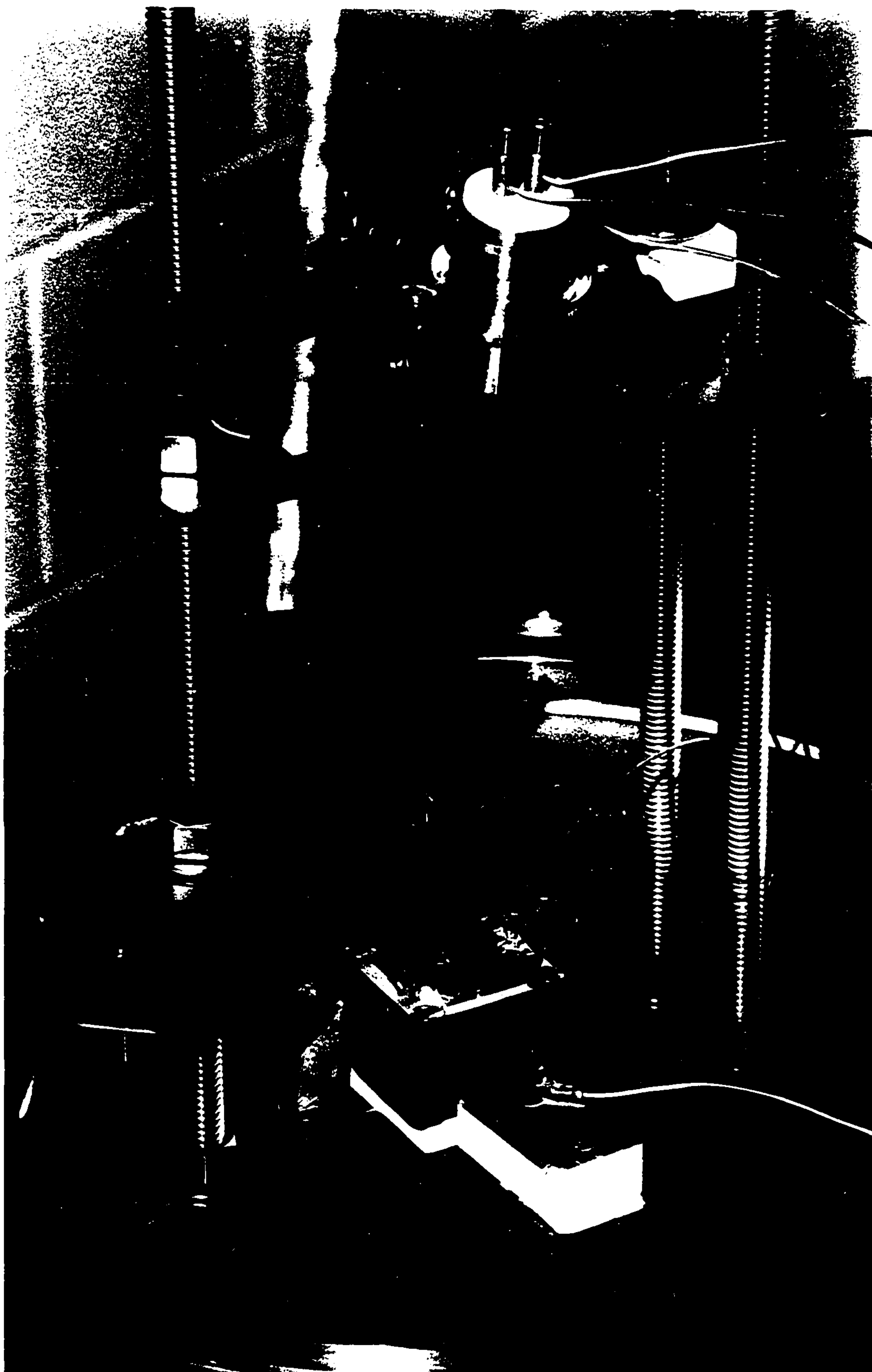

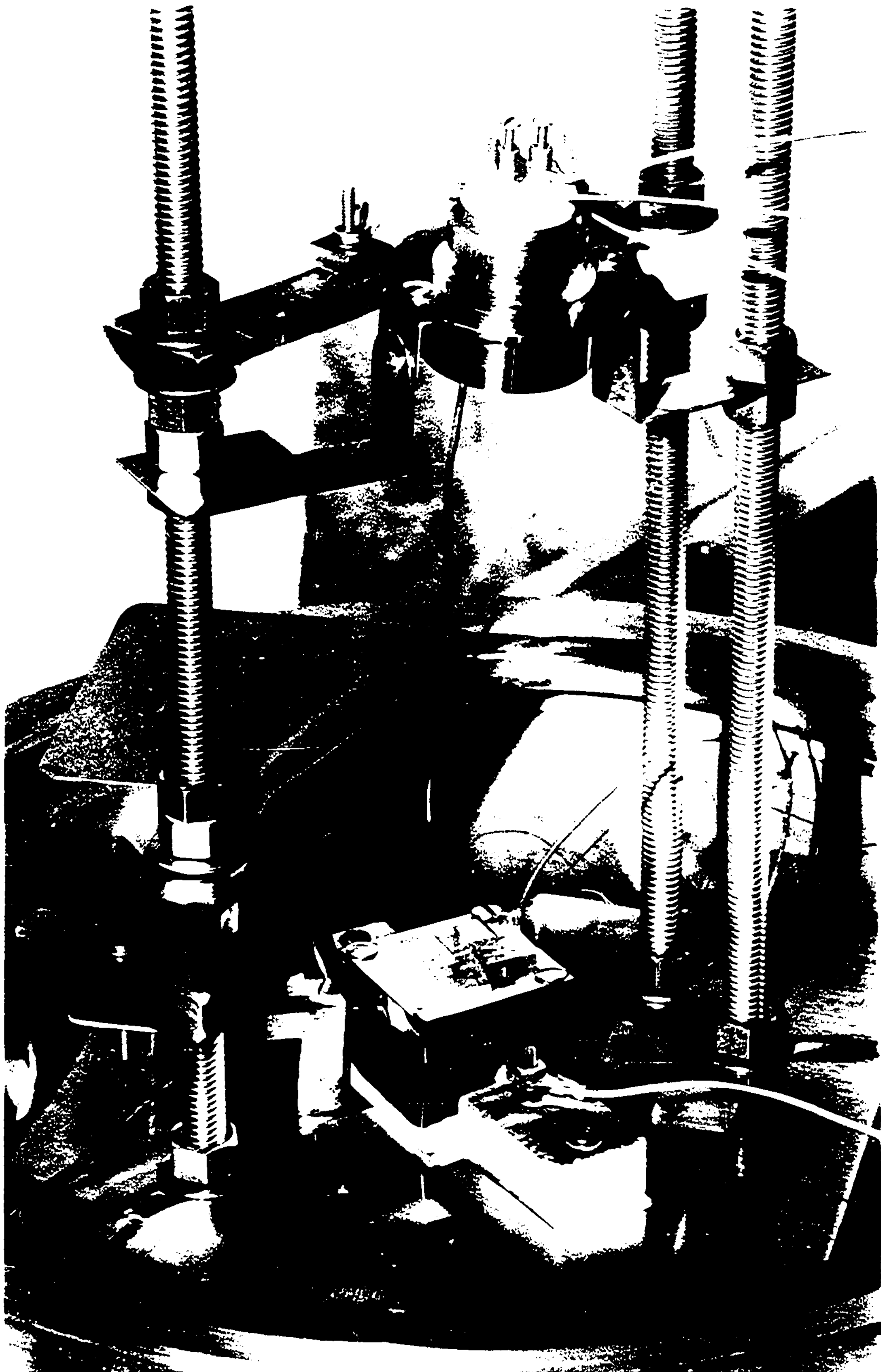

4.1.3 Evaporation Procedure

The substrate must be suitably prepared for evaporation in order to obtain a good epitaxial film. It must be clean, smooth and flat otherwise magnetic discontinuities can occur in films grown on steps of a cleaved surface. Sella and Trillat (1964) have shown by a decoration technique that a freshly cleaved NaCl crystal has a large number of cleavage steps with heights ranging from atomic dimensions to several tens of nanometers. A cleaved surface is therefore far from being plane and it presents a high microrelief.

In this study deposition of the film was carried out simultaneously on four substrates. Three of them, namely (100), (110) and (111) were polished and one was not. The latter was freshly cleaved to expose a (100) surface and was included for comparison. Polishing was done by lapping the crystals on 'selvyt' cloth 'wetted' by 95% alcohol until they were shiny and then followed by quick rinses in 95% alcohol and methanol.

With the substrates ready, the tungsten spiral source in the evaporator was loaded with Ni-Fe wire. The cleaved (100) and polished (100), (110) and (111) NaCl substrates were placed on the substrate heater. Pumping of the chamber was started and the whole system was baked periodically over a period of two weeks to outgas the adsorbed gases from the walls of the chamber until the

residual gas pressure was down to about 2 to 3×10^{-9} torr. With the shutter in place the tungsten spiral was heated just enough to melt the permalloy wire to degas it. Sella and Trillat (1964) have shown that thermal etching becomes rapid and the relief becomes great if NaCl crystals are heated above 400 °C. A maximum temperature of 365 °C was chosen to heat the substrates to outgas them.

After heating for about one hour, thermal equilibrium was reached with the substrates at 365 °C. Irradiation by 1 kV electrons at a current density of about 0.15 mA/cm^2 was begun shortly before the evaporation was started and was continued until completion. The tungsten spiral was heated for evaporation so as to evaporate at a nominally constant rate of 10 nm/min. The pressure during the evaporation was in the range of 9×10^{-9} to 3×10^{-8} torr. After about three minutes the evaporation was stopped and the substrates with films on them were annealed for 1 hour at the deposition temperature. After they had cooled down to room temperature, the substrates were taken out of the evaporator for thickness measurement by X-ray fluorescence and then the films were stripped by floating them off on distilled water to be picked up on 200 mesh copper grids for examination in the electron microscope.

4.2 Thickness Measurement

The thickness of the samples were measured nondestructively by X-ray fluorescence. The standard

for the method was a cover glass placed near the substrates in the evaporation chamber so that the film deposited on it at the same time as the crystals. The film thickness on the cover glass was measured by the Tolansky technique using a multiple beam interferometer attachment to a Leitz microscope.

The NiKα characteristic line intensity excited in the film by X-rays from a tungsten target tube were measured in a Philips PW1040 X-ray spectrometer. After setting the X-ray tube voltage and current at 40 kV and 15 mA, the spectrometer was allowed to warmup for approximately 1 h to reach a steady state condition for X-ray emission and electronic fluctuations. Using a LiF crystal, the X-ray detector was set at 48.66° 2θ to receive NiKα characteristic X-rays. The background count was obtained by using a plain cover glass and a NaCl crystal. In the case of thin films, the spectral line intensity vs. thickness curve is linear for film thicknesses up to at least 500 nm for analytical wavelengths shorter than 0.2 nm. The thickness of the samples were determined from the knowledge of the thickness of the standard and measurement of NiKα intensity from the standard and the sample.

4.3 Electron Microscopy

4.3.1 Transmission and Diffraction Operation

The electron microscope used in this study was a standard 5 lens AEI EM6G microscope. Figure 4.2 illustrates the ray paths used in the modes of microscopy and

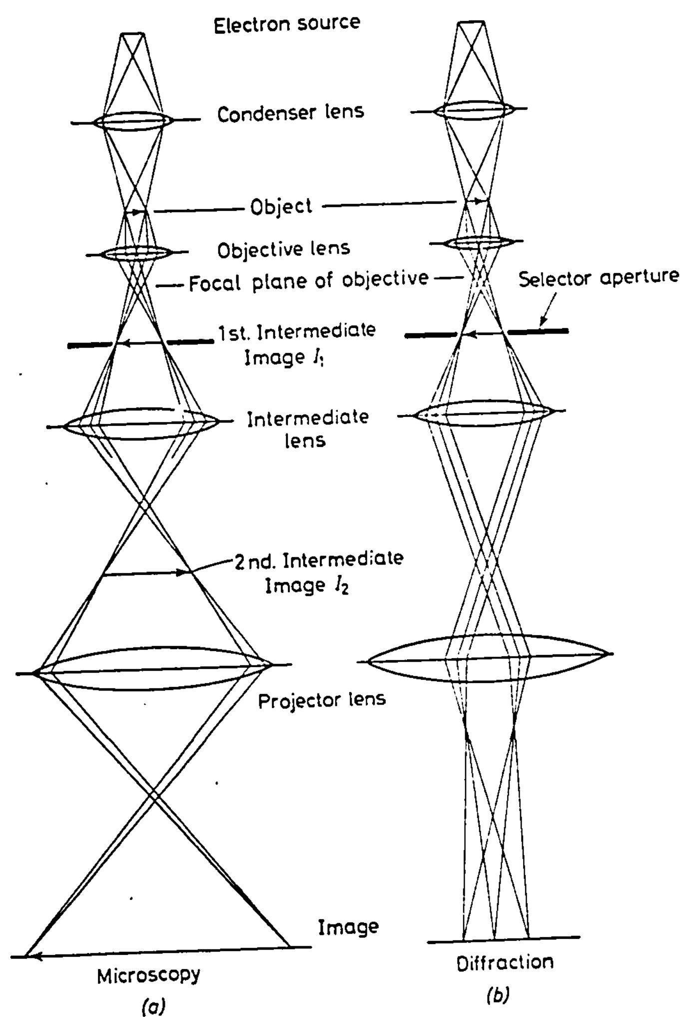

Figure 4.2 Ray paths of (a) microscopy and (b) diffraction in the electron microscope. [After Hirsch et al. (1965)]

diffraction. The illumination source is an electron gun in which the filament is held at -100 kV with respect to the anode. It produces a 50 μm wide crossover in front of the filament which acts as the effective electron source.

The condenser system consists of two lenses which limit the area of the object being illuminated. Condenser 1 is a very strong lens whose function is to produce a highly demagnified image (∿ 1 μm diameter) of the gun crossover. The condenser 2 lens projects this image on to the object plane. By varying the excitation on the second condenser lens, the size of the focussed spot can be varied from 2 to 25 μm. A condenser aperture (∿ 400 μm) is used to limit the angular spread of the beam entering condenser 2 and it defines the illumination aperture ($\sim 10^{-3}$ rad) when the condenser system focusses the electron source on to the object plane.

The third lens is the objective and is the most important lens in the electron microscope. In the normal operation of the microscope, its focal length is 4 mm and it forms a diffraction pattern of the object in the back focal plane. A 50 μm aperture is located in this plane. It produces contrast in the image by stopping out the diffracted electrons. The objective has a magnification of 10× and it forms the first image at the intermediate lens aperture.

The first image is further magnified by the

intermediate lens which controls the total magnification of the instrument. Its focal length can be varied from 5 mm to 50 mm resulting in image magnifications ranging from 1× to 100×. The selector aperture (10 μm) in the first image plane is used to limit the area under observation to 1 μm.

Finally the projector lens with a fixed magnification of 200× forms the image on the fluorescent screen.

The diffraction pattern is obtained by removing the objective aperture and defocussing the intermediate lens to image the pattern in the back focal plane of the objective lens on to the object plane of the projector lens.

4.3.2 Calibration of Image Magnification and Rotation

The magnifications given by the manufacturer for different settings of the intermediate lens current are in error due to variations in high voltage, location of the specimen plane and hysteresis effects in the lenses. An accurate and independent measurement is therefore necessary. Due to their excellent dimensional stability, carbon grating replicas are perhaps one of the best standards available for magnification calibration. A 2160 lines/mm grating from E. F. Fullam, Inc.† was placed in the specimen plane without disturbing the lens currents

† E. F. Fullam, Inc., P. O. Box 444, Schenectady, N. Y.

and a photograph taken whenever an accurate value of magnification was necessary.

Sometimes it is desirable to compare the micrograph of an area with its diffraction pattern. The lenses introduce an inversion and a magnetic rotation the latter being different for micrograph and diffraction pattern. It results from different lens strengths required to form the image and the diffraction pattern. In order to calibrate the relative rotation, a single crystal plate of molybdenum trioxide was used. It is pseudo-orthorhombic and has its long edge parallel to [001] direction. By recording the diffraction pattern and the crystal image on the same plate, the angle between the [001] direction in the crystal and [001] direction in the diffraction pattern can be measured.

4.3.3 Specimen Holder for Lorentz Microscopy

In the normal mode of usage of an electron microscope, the specimen is immersed in the magnetic field of the objective lens pole pieces. The radial component of this field in the object plane can be very high and it exceeds the coercive force of the sample with the result that the domain walls are swept out leaving the film saturated.

In the AEI EM6G electron microscope (Grundy and Tebble 1968), when the objective lens is focussed on the sample placed in its normal position, the field is about 3×10^5 A/m. It drops to 1.6×10^4 A/m about 5 mm above the sample position and focussing the lens on this plane further

reduces the field to 5.5×10^3 A/m which is effectively normal to the plane of the sample.

To image the magnetic domains one therefore uses either the far out of focus mode with the objective lens turned off or the near focus mode with the objective lens excited but the specimen elevated above its normal position. In this study, the near focus mode was employed.

Figure 4.3 illustrates the special shortened specimen holder that was constructed to displace the sample above its normal position. With the insertion of a conical sleeve the upward displacement of the sample was 8 mm. The sample under observation was seated in a threaded insert which could be mechanically moved up or down the sample holder by simply turning it. This facility was used to calibrate the out of focus distance z as a function of the excitation of the objective lens.

A 'holey' formvar film was used as a sample for calibration purposes. As the sample was raised in discrete steps, the objective lens was focussed on it. The current in the objective lens was measured as an iR drop across a 100 Ω standard resistor connected in parallel with the lens coil by a potentiometer and it was plotted as a function of z. Figure 4.4 shows the curve so obtained which is representative of the defocussing conditions for the EM6G microscope. In order to be able to reproduce the same focal length for the same lens current, the objective lens was turned off to make the initial condition the same every time and then its excitation was increased to the required value along

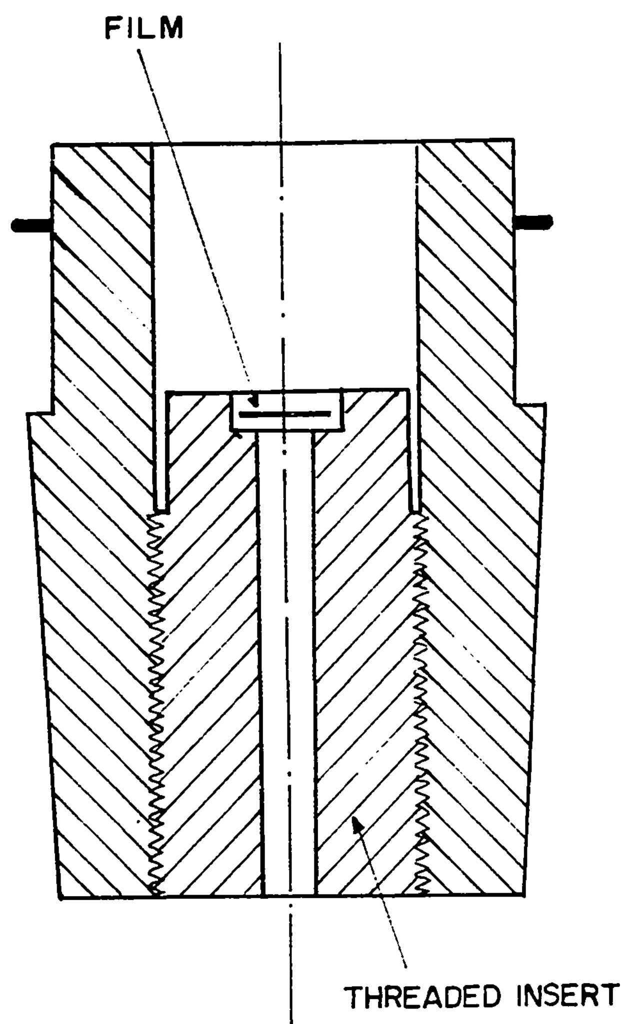

Figure 4.3 The special specimen holder for Lorentz microscopy.

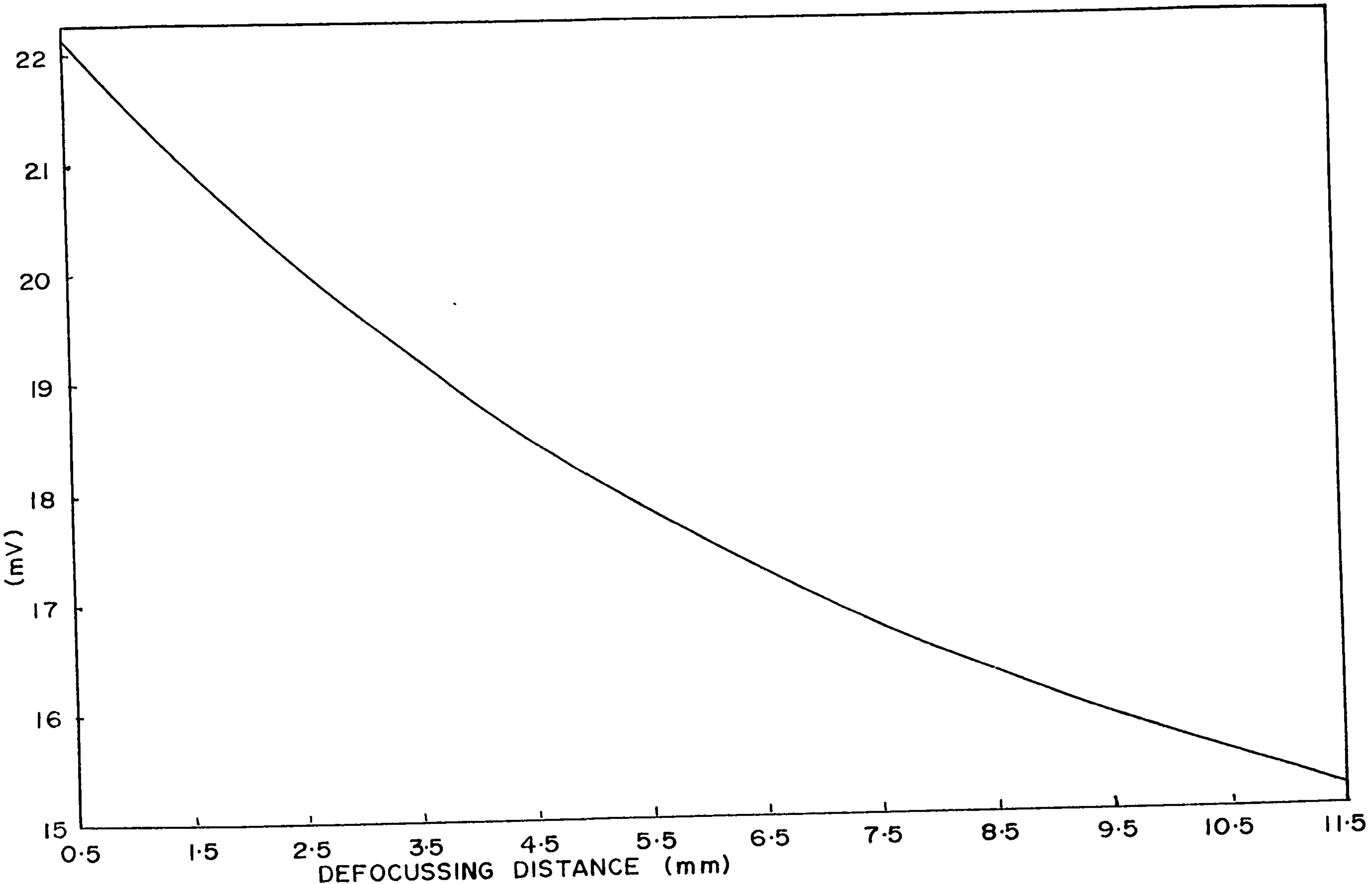

Figure 4.4 Calibration curve for the defocussing distance.

the same direction of a minor hysteresis loop. The intermediate and projector lenses were also cycled along their respective minor loops before setting their currents at their normal levels. The defocussing distance z is measured from an arbitrary origin. By reading off the value of z at focus and at underfocus on the calibration curve, the defocussing distance could be obtained.

4.3.4 Determination of Illumination Aperture

The need for obtaining as small an illumination aperture as possible has been stressed in Chapter 3. It can be achieved by creating a small effective electron source which subtends a small angle at the specimen plane and hence yields a nearly coherent illumination. A small effective electron source was obtained by strongly exciting the condenser 2 lens to demagnify the crossover of the gun. The intensity of illumination varies as the square of the illumination aperture and thus falls off very rapidly. Long exposure times were therefore necessary. However, vibrations of the microscope column limited exposure times to a maximum of 36 sec.

A 'holey' formvar film was used (Hall 1966) to estimate the illumination aperture. It was placed in the raised object plane. With the objective lens slightly out of focus a micrograph of the film was taken. The number of Fresnel fringes at the edges of the holes was counted. From a knowledge of the defocussing distance,

the estimate of the illumination aperture was less than 5×10^{-5} radian.

4.3.5 Small Angle Electron Diffraction

When a beam of electrons is transmitted through a ferromagnetic film, it is deviated by the internal field of the film. If the illuminated area in the film contains a π rad domain wall, the central spot is split into two subsidiary spots. The maximum angular deviation ϕ_m called the Lorentz deflection is about 10^{-5} radian. Such small deviations cannot be resolved from the direct beam when the electron microscope is used in the normal diffraction mode in which the camera length L is about 0.4 m. It produces a separation of 4 μm on the plate between the undeviated spot and the deflected spot. A solution for this problem is to use the microscope as a small angle diffraction camera in which the camera length can be increased by several orders of magnitude.

The ray diagram of the electron microscope for the very long camera length method (Blackburn et al. 1969) is illustrated in Figure 4.5. In this method all the five lenses are used. The condenser 1 and condenser 2 lenses are overfocussed to reduce the beam divergence. It produces a small effective source with an illumination aperture of about 10^{-6} radian which is more than enough to resolve the 10^{-5} radian Lorentz deflection. The objective lens is excited very weakly to produce the

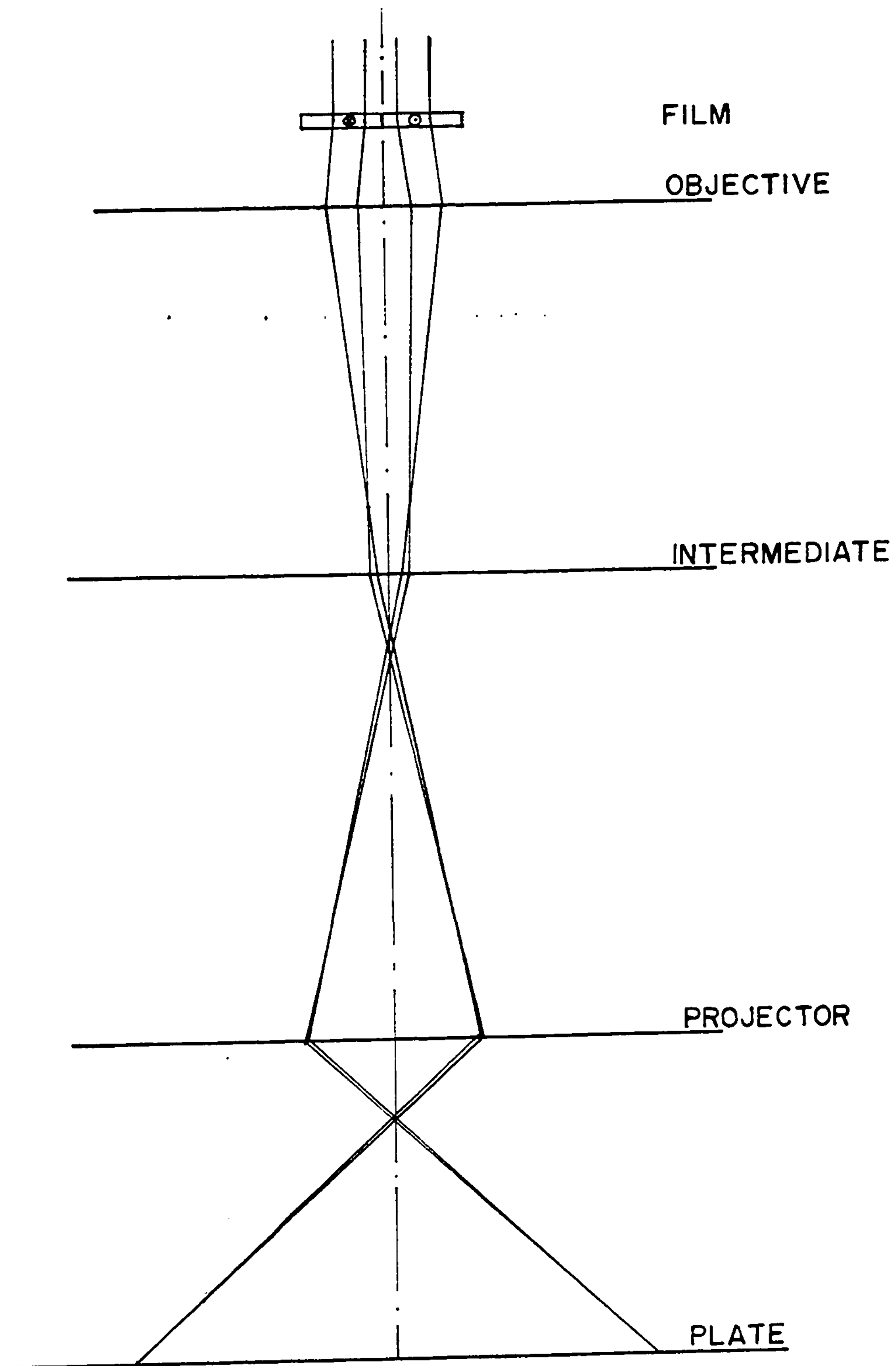

Figure 4.5 Ray diagram of the electron microscope when it is used as a small angle electron diffraction camera.

diffraction pattern in the selector aperture plane. Since it was not possible to reduce the objective lens current using the front panel controls, an attennuator was built in to do it. The intermediate and projector lenses produce a magnified image of the pattern at the photographic plate. Specimen area selection can be made by the objective aperture.

The effective camera length L is given by

$$L = l\, M_I\, M_P$$

where l is the distance from the objective lens to the selector aperture and M_I and M_P are the magnifications of intermediate and projector lenses respectively. An estimate of L from the physical dimensions and magnification factors of lenses is not reliable. In practice instead of measuring L directly it is measured as a product $L\lambda$ -a constant for the given experimental setup using a suitable calibration specimen. Figure 4.6(a) shows the diffraction pattern obtained using a 2160 lines/mm carbon grating replica. About 6 orders of diffraction beams on both sides of the primary beam can be seen. From the formula

$$L\lambda = rd$$

(a)

(b)

Figure 4.6 (a) Small angle diffraction pattern from a 2160 lines/mm carbon grating replica (b) Splitting of a spot in the diffraction image due to Lorentz deflection of the electrons in the permalloy film.

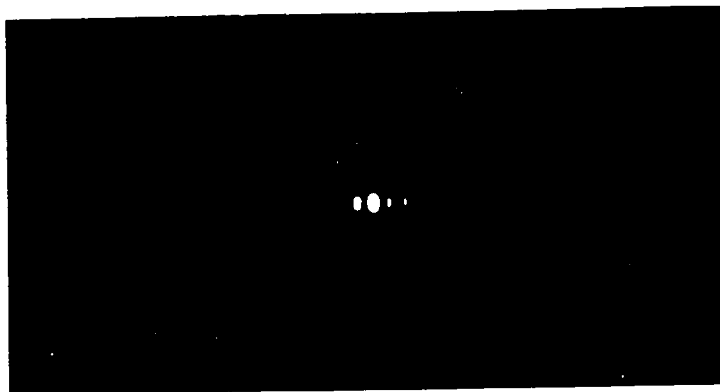

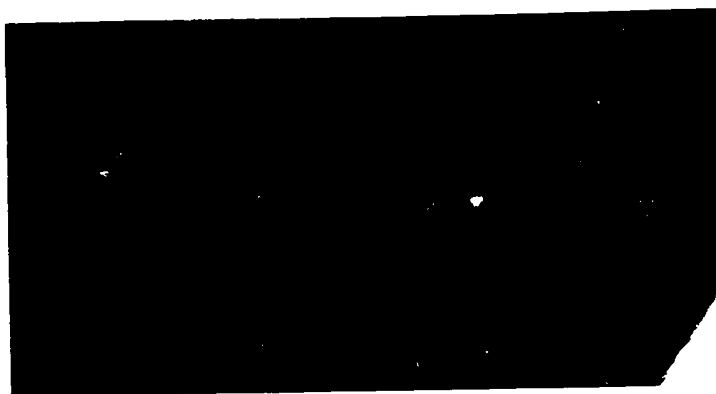

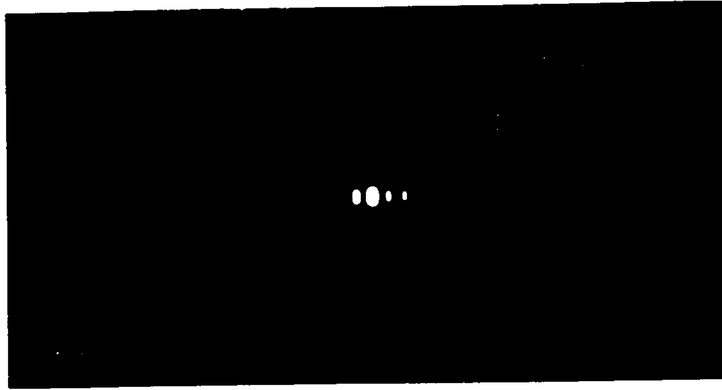

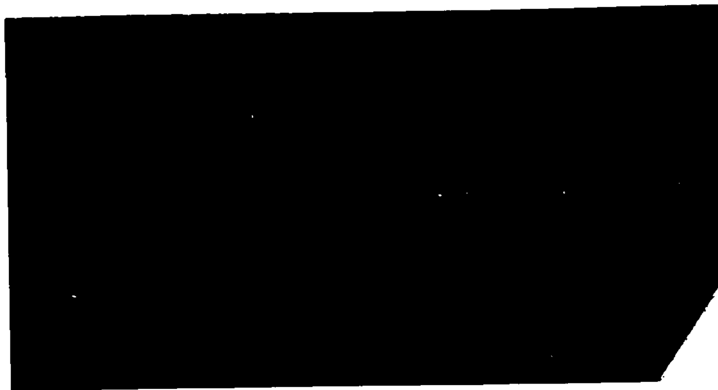

where d is the grating constant and 2r the separation between the two spots, the camera constant can be obtained. A typical value of $L\lambda$ in this mode of operation is 0.536×10^{-9} m^2 which for an electron wavelength of 3.7 pm gives for L a value 145 m. This large value is due to the long focal length of the objective lens. Using this value of $L\lambda$ in equation (3.39) the value of J_s can be determined from a knowledge of film thickness and Lorentz spot separation. Figure 4.6(b) shows the split spots.

4.3.6 General Experimental Procedure

The films used in the domain wall width measurements were first demagnetized by applying alternating current demagnetization to introduce domain walls and then were examined in the microscope. The small illumination aperture of less than 5×10^{-5} radian necessitated exposure times of atleast 36 seconds.

After initializing the objective lens to the condition that prevailed during the calibration of the defocussing distance, the objective lens was defocussed by varying its current along the same direction of the minor loop as was done during its calibration. For each film sample about 8 plates were taken at different defocussing distances. The contrast for z upto 4 mm was so poor that no meaningful measurements could be made. The wall widths were then obtained from least square fits to the data points obtained from microphotometry.

For the measurement of the magnetic polarization J_s, the calibration grating was inserted into the microscope immediately after the split spot pattern was recorded. Care was taken to make sure that the position of the grating in the microscope column was as close as possible to that of the sample. No lens trimming was attempted to improve the focus of the diffraction pattern.

4.4 Microphotometry

The domain wall widths in the electron micrographs were measured using a Jarrell-Ash recording microphotometer. The slit width and length used were 10 μm and 2500 μm respectively. The plates were scanned perpendicular to the divergent wall direction at a rate of 1 mm/min making sure that the long side of the slit was parallel to the wall. About 10 to 13 separate scans were made along each wall. The half widths were obtained from the microphotometer traces using the plate magnification, scan rate and chart speed. Noise in the traces was mainly due to magnetization ripple. A typical trace is shown in Figure 4.7.

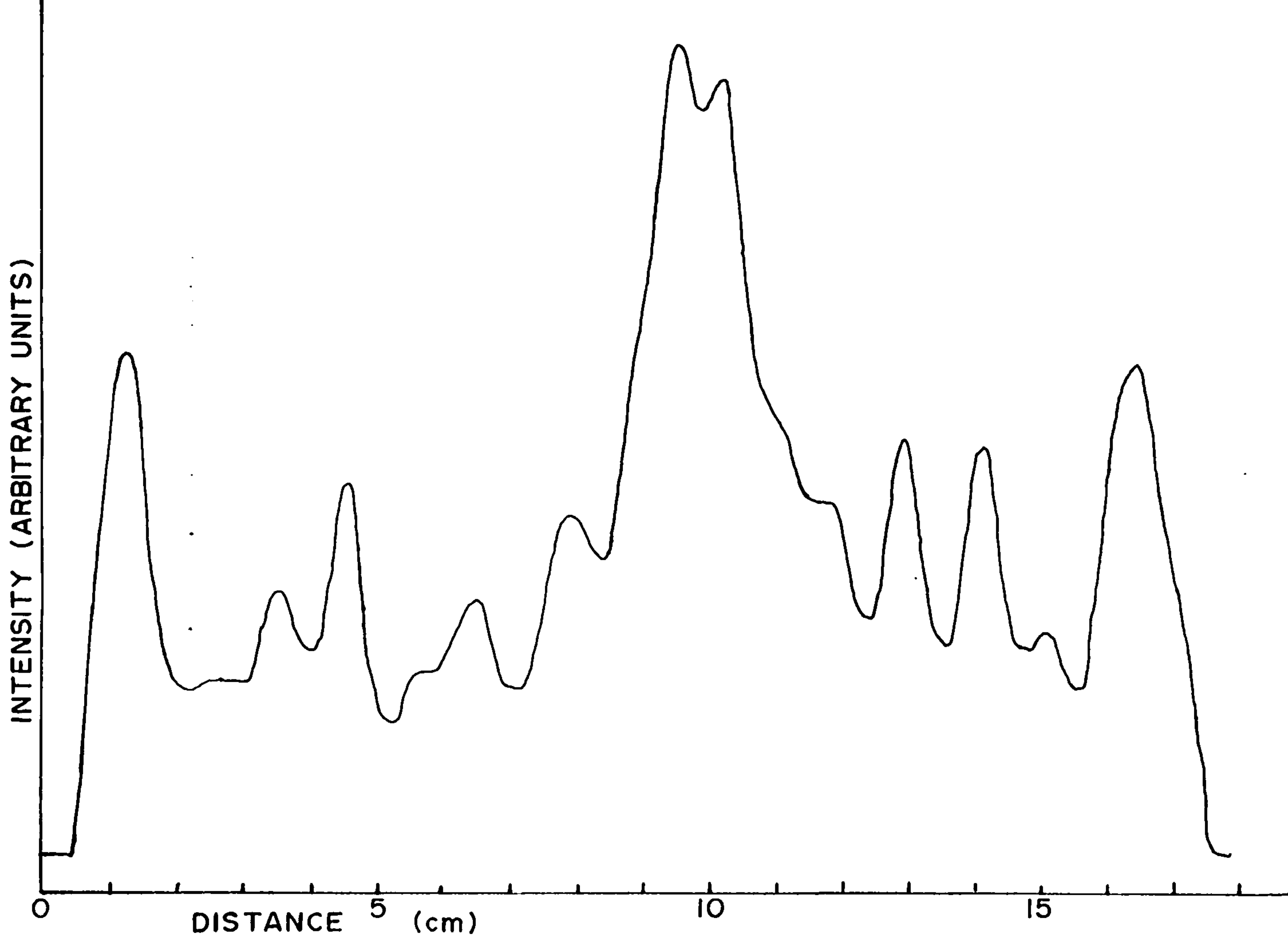

Figure 4.7 A typical photometer trace across a domain wall (z = 4.25 mm).

CHAPTER 5

RESULTS AND DISCUSSION

5.1 Film Structure

Epitaxial films of permalloy deposited at 365 ^{o}C on freshly cleaved (100) and polished (100), (110) and (111) faces of NaCl have been obtained. Figures 5.1 through 5.4 show the electron micrographs and electron diffraction patterns of the films obtained. In the figures, the upper pair are of films obtained without electron bombardment and the lower pair with simultaneous electron bombardment.

The electron diffraction patterns show that the non-bombarded films are on the average partially oriented polycrystalline films whereas the bombarded ones are better oriented. There is however a tendency in both types of films to grow in parallel orientation to that of the substrate. Most of the non-bombarded films contain other orientations in addition to the parallel orientation. It is a result of the symmetry relation

(a)

(b)

0.1 μm

(c)

(d)

0.1 μm

Figure 5.1 Transmission electron micrographs and diffraction patterns of permalloy evaporated onto cleaved (100) NaCl. (a) and (b) with no electron bombardment. (c) and (d) with simultaneous electron bombardment.

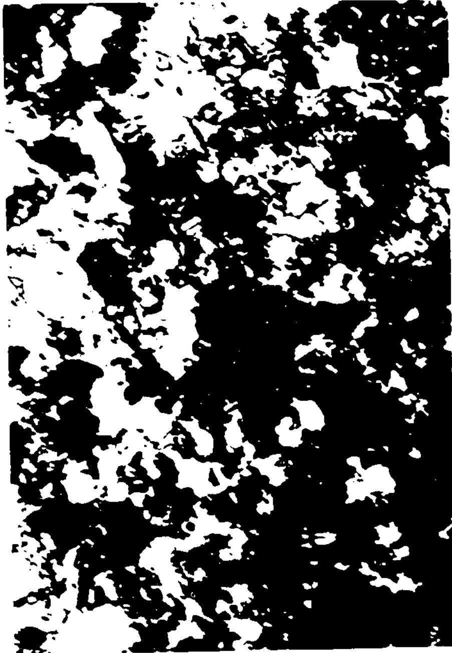
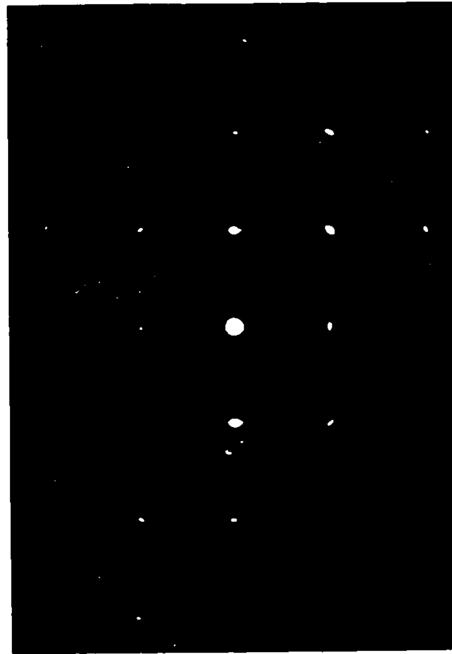
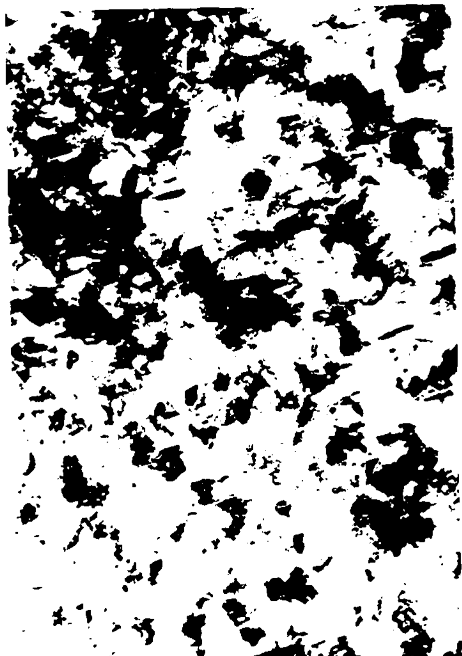

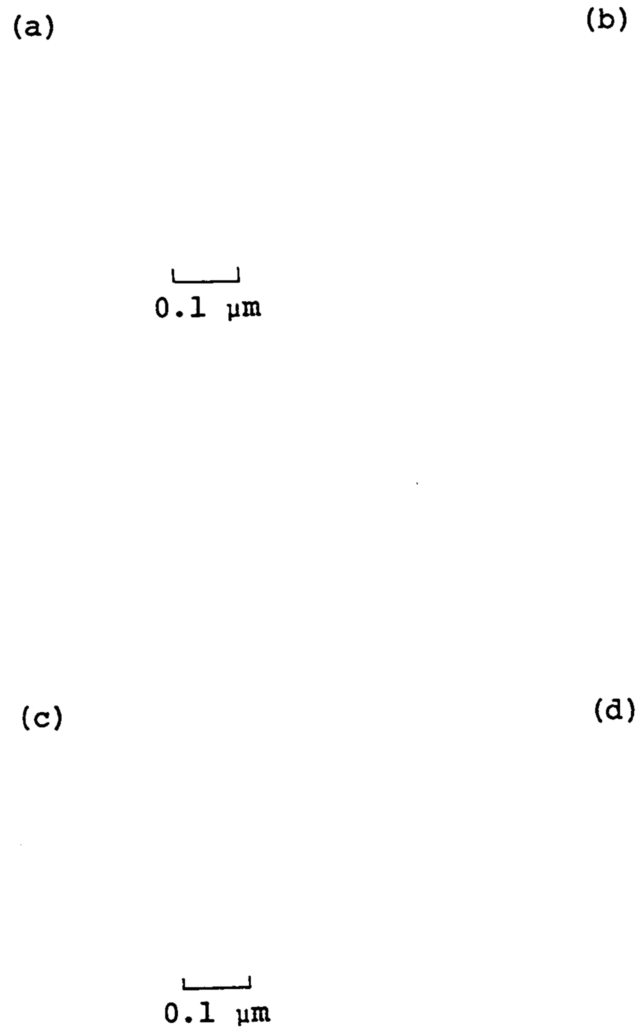

Figure 5.2 Transmission electron micrographs and diffraction patterns of permalloy evaporated onto polished (100) NaCl. (a) and (b) with no electron bombardment. (c) and (d) with simultaneous electron bombardment.

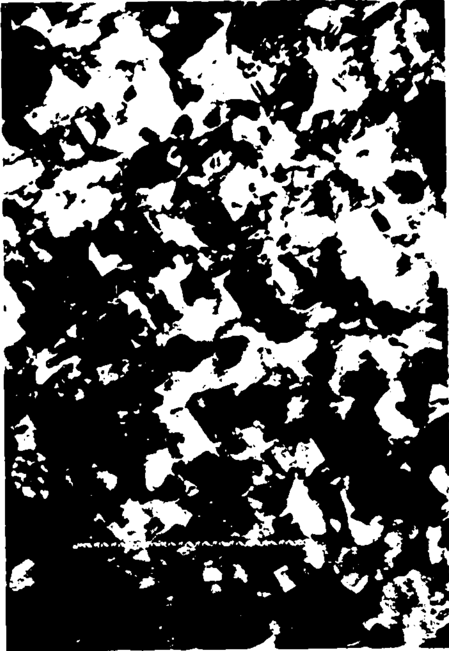

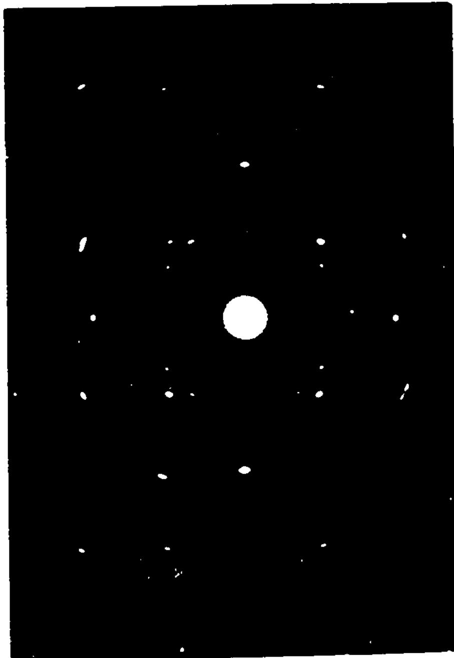

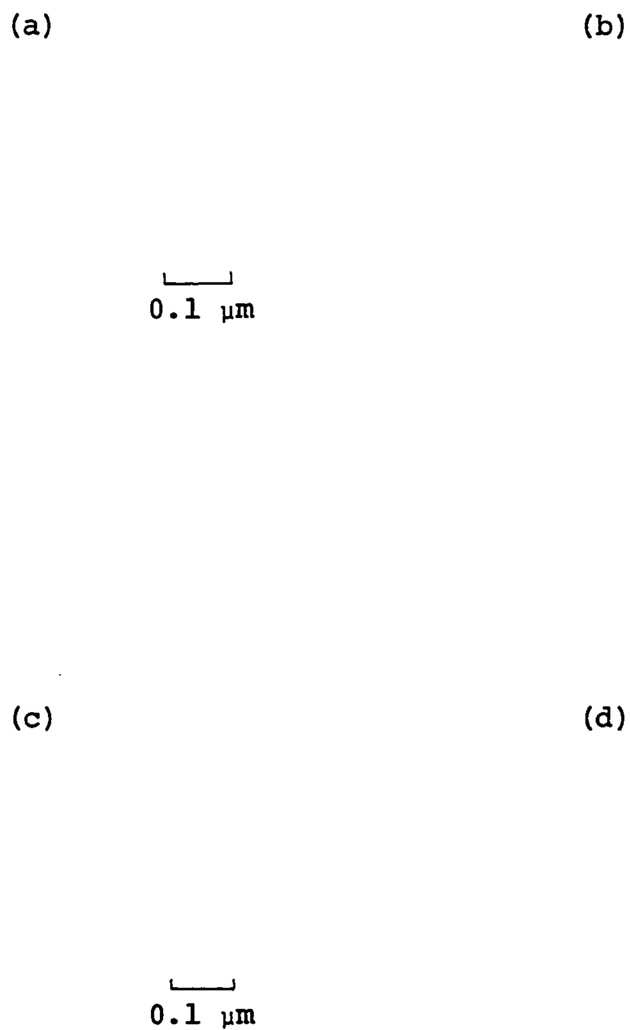

Figure 5.3 Transmission electron micrographs and diffraction patterns of permalloy evaporated onto polished (110) NaCl. (a) and (b) with no electron bombardment. (c) and (d) with simultaneous electron bombardment.

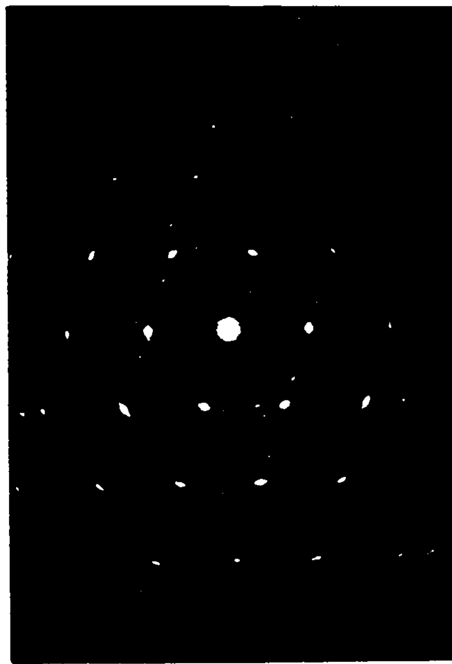

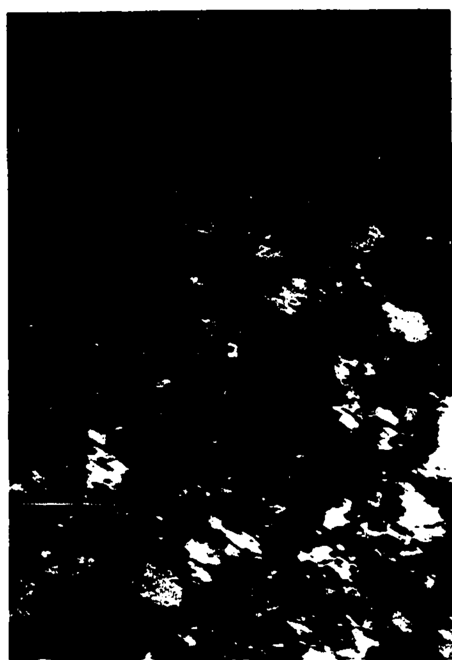

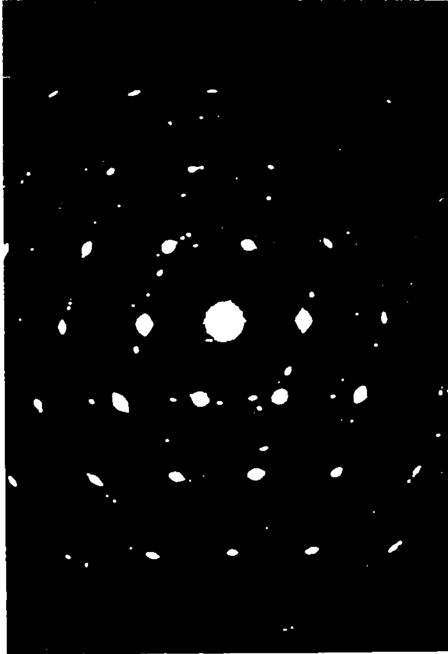
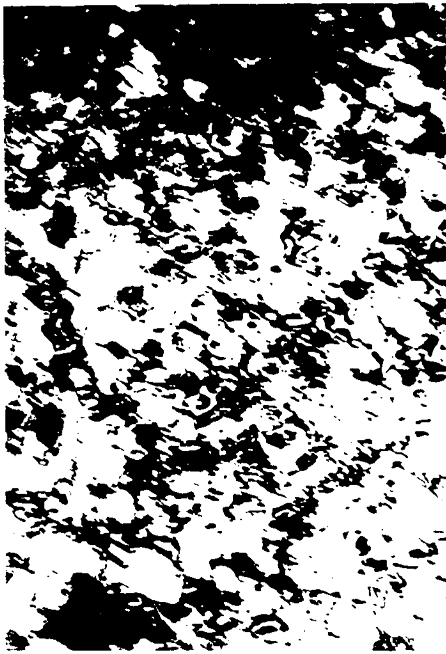
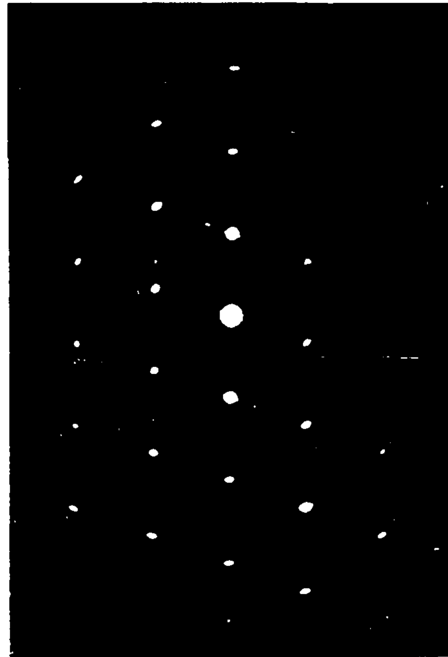

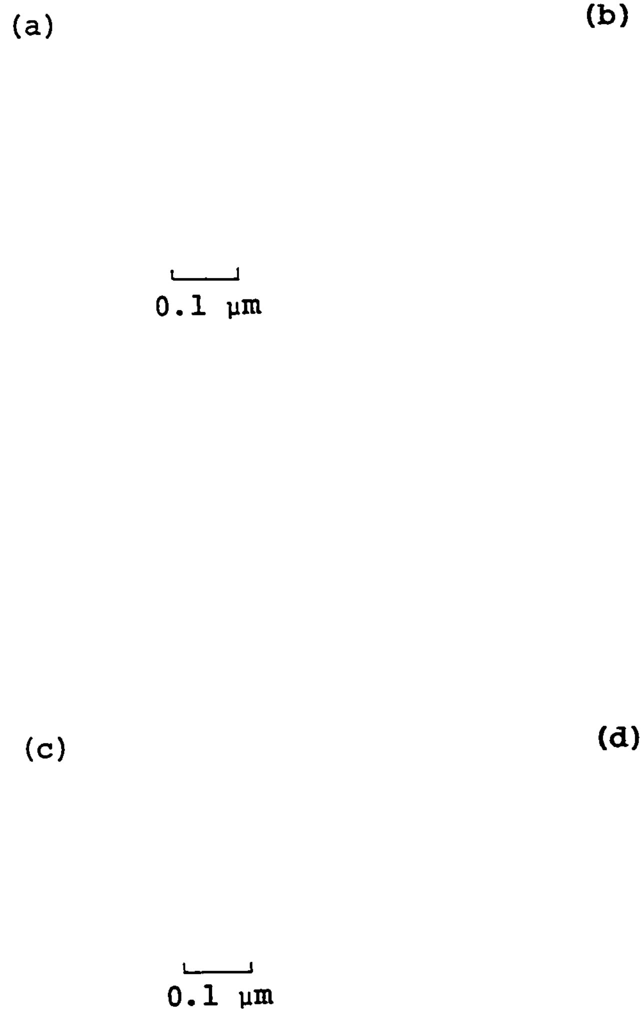

Figure 5.4 Transmission electron micrographs and diffraction patterns of permalloy evaporated onto polished (111) NaCl. (a) and (b) with no electron bombardment. (c) and (d) with simultaneous electron bombardment.

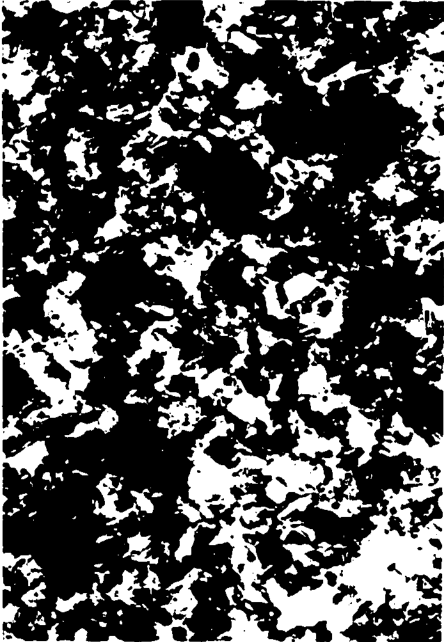

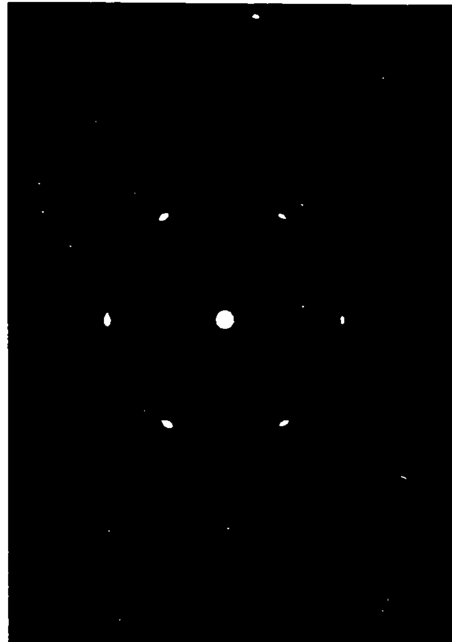

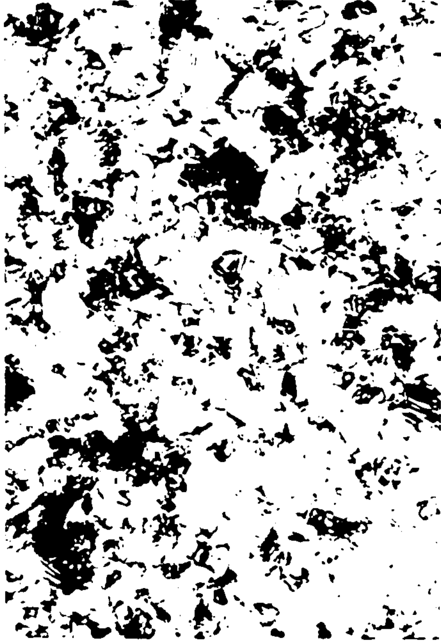

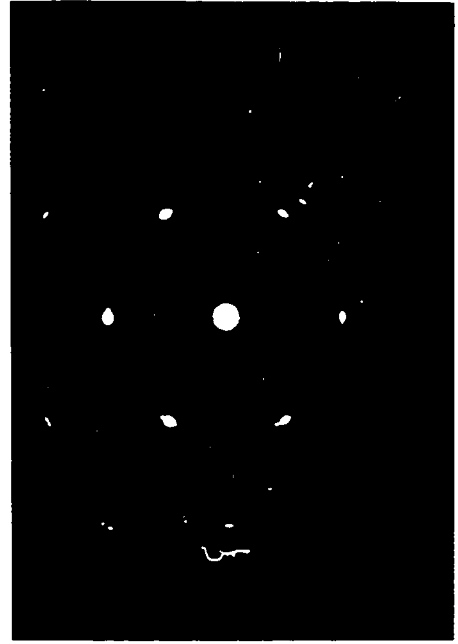

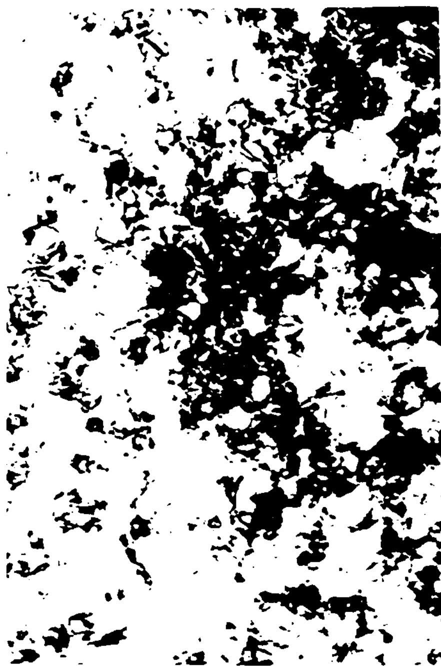

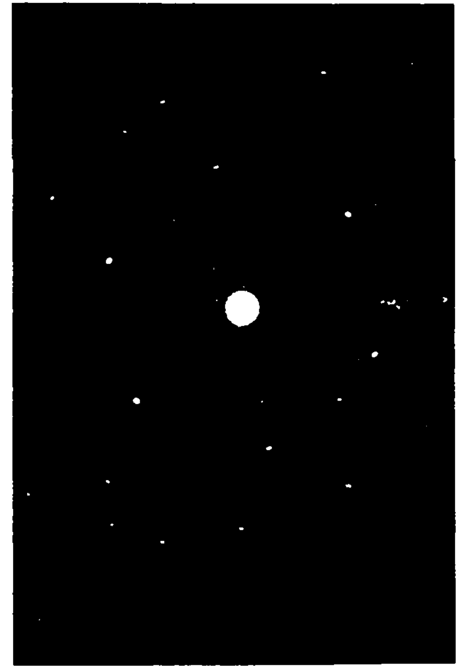

between the deposit and the substrate which causes multiple positioning and is observed frequently in fcc films grown on NaCl. The spots also show arcing due to the presence of areas in the film whose orientation deviated from the preferred one by a rotation about the normal to the specimen plane.

The diffraction patterns of the non-bombarded films exhibit spot patterns superimposed on faint polycrystalline rings whose intensity is much less than that of the spots. These rings arise from the presence of randomly oriented crystallites in the film. The electron bombarded films produced only spot patterns showing that the orientation had improved significantly. Their spots were also less arced. In addition to the regular spot patterns, there are extra reflections visible in the diffraction pattern. These extra spots are particularly noticeable in the (110) films (see Figure 5.3) and arise as a result of the presence of twins. The micrographs also reveal a large number of stacking faults and twins. Such structural defects were present in both the electron bombarded and non-bombarded films.

The crystallographic direction in the electron bombarded films changed very little over more than five squares in a 200 mesh copper grid. However, there was a change over larger distances and it is probably due to

wrinkling of the films. It is interesting to note that the orientation of the film deposited on a cleaved (100) NaCl was better than that grown on the same polished face. This is contrary to what Heavens et al. (1961) observed in their films which were grown under poorer vacuum conditions than ours.

The presence of a high density of structural defects such as stacking faults and twins in our films is in agreement with the results of others (Burbank and Heidenreich 1960, Schoening and Baltz 1962). Epitaxial films of fcc metals grown on NaCl are known to twin on all the four {111} planes. Structural defects have also been observed in epitaxial films of permalloy by Collins and Heavens (1957), Heavens et al. (1961), Burbank and Heidenreich (1960), Schoening and Baltz (1962), Alessandrini (1966) and Yelon et al. (1965). It is difficult to remove such defects by annealing the films in vacuum. Schoening and Baltz annealed their partially monocrystalline films by electron beam heating in the microscope. It resulted in a perfect (100) orientation film with a high percentage of {111} twins. Alessandrini annealed her films at 450 ^{o}C for 4 h in a 10^{-7} torr vacuum. The film developed a second orientation with a {111} texture. When Heavens et al. annealed their films in 10^{-5} torr vacuum for 2 h at 1000 ^{o}C the orientation deteriorated. Burbank and

Heidenreich estimated that about 30 to 40% of their film was twinned. They suggest that since there is rarely an integral lattice vector between coalescing nuclei a boundary of high energy will be formed between coalescing nuclei. The strain energy that accumulates as a result is thought to provide the driving force for the occurrence of faulting, twinning, recrystallization or other relief processes.

It has been thought for some time that the nucleation and only this porcess determines the epitaxial orientation of a continuous film on a substrate. The recent work of several authors (Pashley 1959, Matthews 1960, Matthews and Allinson 1963) has shown that the initial nuclei need not be in parallel orientation to produce a continuous epitaxial film. From the general result that the alignment of a film improves as its thickness increases, it can be concluded that the processes that take place during post nucleation growth can cause the orientation of the initial deposit to be altered substantially. For example, polycrystalline films formed on an amorphous substrate develop a preferred orientation during growth.

The work of Basset (1960), Pashley et al. (1964), Pashley (1965), Matthews (1965b) and Matthews and Grunbaum (1964, 1965) has shown that appreciable orientation changes do occur when two slightly misoriented nuclei coalesce

resulting in the rotation of one nucleus into the orientation of the other. Rotations of up to 10^{0} are possible and are about an axis perpendicular to the film plane. Such changes therefore have a profound effect on the final orientation of the film.

When two islands coalesce, the tendency is for the smaller of the two islands to rotate into the orientation of the larger one resulting in an improvement in orientation for two reasons. Firstly the larger nuclei are on the average better aligned than the smaller ones and so upon coalescence the smaller nucleus rotates into perfect alignment. Secondly a rotation into the orientation of the better aligned of the two nuclei rather than away from it results in a reduction of the interfacial energy. Therefore for the final film to be oriented perfectly, two requirements must be satisfied. The first requirement is that the perfectly aligned nuclei must grow faster than the non perfectly aligned nuclei resulting in bigger epitaxially oriented nuclei. The second requirement is that the density of the islands should be large enough to result in an early coalescence before the misaligned nuclei grow bigger than a critical size at which reorientation is not possible.

On the basis of the foregoing reasoning Matthews (1965a) attempts to explain the poor orientation of

epitaxial films grown in ultra-high vacuum on vacuum cleaved NaCl compared to the better orientation of the same films grown on NaCl cleaved outside the vacuum evaporator. The density of initial nuclei on the clean UHV cleaved NaCl is low. About 10% of these nuclei are in (111) orientation with the rest in (001) orientation. As more film material is added, the (111) nuclei tend to grow more rapidly than the (001) nuclei with the result that they will be bigger at the time of coalescence. The bigger (111) nuclei consume the smaller (001) nuclei resulting in the predominance of (111) orientation of thicker films. On the other hand when an air contaminated NaCl is used as the substrate, the initial density of nuclei is high. The coalescence of islands occurs before (111) nuclei have a chance to grow bigger resulting in the consumption of (111) nuclei by (001) nuclei. When continuity is established in the film, it will be in (001) orientation. Therefore the initial island density has a controlling influence on the final film (Matthews 1965a).

The result that the cleaved NaCl substrate produced a better oriented (100) film [Figure 5.1(b)] than the polished NaCl [Figure 5.2(b)] can be explained by the same reasoning. It is known that the surface of a freshly cleaved NaCl is not smooth and has a large number of cleavage steps of atomic height and various types of atomic defects (Chopra 1969). Also the cleaving process leaves a

fine dust on the surface of the salt which is not easily removed (Chopra 1969). These steps, atomic defects and dust may act as nucleation centers resulting in an increase in island density producing a well oriented continuous film.

The coalescence phenomenon has a profound effect on the structure and properties of the resulting film since recrystallization, grain growth, orientation changes, incorporation and removal of structural defects etc. occur as a consequence of coalescence. The stage at which coalescence takes place depends on the shape of the nuclei and on the number of nuclei generated per unit area. It therefore depends on the contact angle of nuclei, deposition rate, substrate temperature, contamination and defects on the substrate surface. The dynamics of coalescence is not completely understood at present. Coalescence can be induced at an early stage of the film growth by methods such as the lateral application of an electric field on the substrate (Chopra 1966), irradiation of the substrates by electrons (Stirland 1966, Hill 1966) or X-rays (Inzuka and Ueda 1968) and by ultrasonic agitation (Chopra and Randlett 1967) of the substrate.

It is well known that nucleation on a substrate is enhanced by the presence of surface defects. Since alkali halides are susceptible to electron irradiation damage, they form convenient substrates for electron irradiation

induced early coalescence. Stirland (1966) observed that single crystal films of Au in parallel orientation on vacuum cleaved rock salt are produced at substrate temperatures of 150 ^{o}C if the rock salt is bombarded with 90 V electrons at rates of 10^{13} electrons/cm^{2}/sec. He found that the bombardment increased the initial island density by producing a large number of smaller islands. The bombarded film was predominantly (100)[110] Au || (100)[110] NaCl whereas the non-bombarded film had in addition to the parallel orientation, several others such as (111)[110] Au || (100)[110] NaCl. He was not clear whether this condition alone was sufficient to account for the influence of the bombardment. Later work (Stirland 1967/68) showed that the saturation island density is higher for the bombarded substrate. He also found that bombardment of the substrate during the initial period of evaporation until a 1 nm thick film was formed was sufficient to produce epitaxy in a 30 nm film.

Similar improvement in the orientation of films due to electron bombardment has been observed for various electron energies and fluxes on NaCl and other substrates. For example, Palmberg et al. (1967a, 1968) bombarded 40 V electrons on KCl at 80 ^{o}C (10^{16} electrons /cm^{2}/sec). But Chambers and Prutton (1967a, b) used relatively high energy electrons ($\sim$7 kV) for the deposition of Ni on (100) NaCl and LiF which were heated to temperatures in the

region of 300 to 380 °C. The electron flux was 5×10^{14} electrons $/cm^2/sec$. Nickel films grown on air cleaved NaCl produced a (100) spot pattern along with twinning reflections in the microscope. Vacuum cleaved NaCl produced a film in (100) orientation with no twinning. Kunz et al. (1966) also used high energy electrons (10 to 20 kV, $< 10^{-6}$ A/cm^2) for the deposition of Au on NaCl. They observed the following effects: (1) roughening of the alkali halide substrate surface, (2) an increase in particle density and surface coverage and (3) a change in orientation. The electron irradiation favored the formation of (100) orientation. Lewis and Jordan (1970) used 240 V electrons at rates of 10^{15} electrons$/cm^2/sec$ on vacuum cleaved NaCl. The substrate temperatures used were 30 to 300 °C. They found that films produced by bombardment showed parallel orientation for substrate temperatures as low as 55 °C. The non-bombarded films were polycrystalline at these temperature but had mixed orientation at 300 °C.

Palmberg et al. (1968), Stirland (1969), Chambers and Prutton (1967a, b) and Kunz et al. (1966) conclude that irradiation produces surface defects which act as nucleation centers strongly favoring parallel orientation for the nuclei. These nucleation centers are probably halide vacancies whose electrostatic charges are responsible for trapping the adatoms. The increase in nucleation

density due to electron bombardment has been estimated to be roughly an order of magnitude (Lewis and Jordan 1970).

Chambers and Prutton (1967a, b) suggest that the defects are F centers in simple or agglomerated forms. Others have also attributed the improvement in epitaxy to F centers produced by electron bombardment (Lord 1971, Kunz et al. 1966) and other complex centers (Stirland 1966, 1969; Chambers and Prutton 1967a, b). Recent work employing LEED, Auger Emission Spectroscopy and mass spectrometry suggest that such surface defects are produced by electron bombardment and are responsible for improvement in epitaxial orientation (Chambers and Prutton 1967a, b; Palmberg and Rhodin 1968; Palmberg et al. 1968; Gallon et al. 1968).

The experimental fact that improvements in epitaxial orientation has been achieved in thin films by bombarding the substrate with electrons of various energies and fluxes seems to suggest that its effect is substantically independent of flux and energy. Above certain threshold levels of electron energy and flux which depend on the type of substrate and its temperature, improvement in orientation is produced.

In addition to an increase in island density which improves epitaxy, the electron bombardment seems to cause an improvement in the initial alignment of nuclei also. This inescapable conclusion stems from the fact that

parallel orientation has been obtained at low substrate temperatures. For example, Lewis and Jordan (1970) and Palmberg et al. (1968) have observed epitaxy at 55 ^{o}C and 80 ^{o}C respectively. Palmberg et al. suggest that electron induced epitaxy occurred through an improvement in orientation of the initial nuclei since the recrystallization of misaligned nuclei by coalescence into an epitaxial orientation was unlikely at the low temperatures at which epitaxy was obtained.

Since the higher nucleation density has been attributed to the formation of color centers and it requires 15 keV to produce F-centers in bulk NaCl, electrons of low energy do not at first sight seem to be able to produce them in NaCl eventhough Stirland was successful in obtaining parallel orientation using 90 V electrons. Chambers and Prutton (1967a, b) see no contradiction in this since a cleaved surface is likely to contain many point defects and the creation of an F-center in an already existing vacancy is about 70 to 90 eV. Therefore F-centers and groups of F-centers can be produced according to them at low electron energies. In our experiments, we used 1 kV electrons to bombard the NaCl substrates. It is reasonable that the above explanation for the production of color centers in our substrates also holds.

It is known that many of the defects are annihilated by recombination processes in a hot substrate.

Therefore electron bombardment would not be expected to influence the orientation of the deposit if the evaporation takes place after the thermal removal of the defects. This probably explains why experimentally it is found that deposition after bombardment does not give epitaxy (Stirland 1967/68). However a simultaneous bombardment of the substrate and deposition (Stirland 1966) does,suggesting that a steady state concentration of defects due to the production and thermal annihilation is sufficient to induce epitaxy (Palmberg et al. 1968). In our experiment, we bombarded the NaCl substrates held at 365 $^{\circ}C$ with 9×10^{14} electrons/cm^2/sec. At higher temperatures vacancy clustering may also take place so that nucleation may not be at single vacancy sites.

Since the experimental results published in the literature shows that electron irradiation favors (100) orientation of films on (100) NaCl, and we find improvement in orientation on (110) and (111) faces of NaCl also, it is conceivable that the same processes that are responsible for improvement in orientation on (100) NaCl are responsible for similar improvement on (110) and (111). Electron irradiation seems to improve epitaxy for the following reasons. It promotes epitaxial orientation of initial nuclei and it further causes early coalescence and recrystallization by increasing the initial island density. The irradiated surface is a complicated resultant of induced

dissociation, desorption, bulk-to-surface diffusion which are strongly dependent on substrate temperature, bombardment flux and energy (Chambers et al. 1970). The precise nature of the process is still unknown.

5.2 Measurement of Magnetic Polarization

The thickness of the films measured by Tolansky and X-ray techniques and magnetic polarization (J_s) measured by using the electron microscope in the small angle diffraction mode are summarized below.

Film	Thickness (nm)	J_s (T)	% difference from bulk value
(100) cleaved	33	0.926	7
(100) polished	29	0.861	13
(110) polished	31	0.875	12
(111) polished	33	0.896	10

Table 5.1 Summary of measured film thickness and magnetic polarization.

The last column gives the percentage difference of the measured J_s from that of the bulk 82 permalloy which is 0.990 T (Bozorth 1951).

The measured values of J_s were always lower than the bulk value with the percentage difference lying in the range 7 to 13. Similar discrepancies between the measured and bulk values have been reported by Ferrier (1964) and Ferrier and Wade (1964) in the case of polycrystalline films of Fe, Ni and permalloy and by Mader and Nowick (1968) who studied amorphous and polycrystalline films of Co-Au alloys. Ferrier and Wade found deviations of up to 75% with the largest discrepancies in the case of films deposited at the lowest temperatures. Their vacuum (10^{-5} torr) was poor compared to the present work. Mader and Nowick worked in better vacuum conditions (10^{-7} torr) and found 15 to 20% discrepancy. Within experimental uncertainty they found no difference in the value of J_s for amorphous and crystalline films of Co-Au.

From the best experimental work, it is known that J_s does not decrease with decreasing film thickness until the thickness is less than 2 or 3 nm. The concept of thickness loses its meaning below this value as the film becomes granular and no longer has a plane surface. Uniformly plane films of permalloy that were deposited epitaxially on epitaxial films of copper which were in turn grown on mica showed that the value of J_s was closer to bulk up to 0.7 nm (Cohen 1969).

The error in the measurement of J_s can arise from the error in thickness measurement (about 15%) and in estimating the separation of split spots (about 5%). In addition there

are three more sources of error. It has been assumed that J_s lies in the plane of the film due to shape anisotropy. This assumption is quite valid in the case of permalloy films studied here as at this composition, the magneto-crystalline anisotropy is very small. The second is the assumption of bulk density in the film. Since the films were deposited under ultra high vacuum conditions the amount of gases trapped is very small justifying the assumption of bulk density in the films. Finally the existence of demagnetizing field in the space above and below the film can act to decrease the deflection of electrons passing through.

Our non-destructive method of measuring the thickness of the films used in measuring J_s is more reliable than that of others. The usual practice of most workers in thin films is to measure the thickness of the film deposited simultaneously on a monitor glass slide and to assume that it is the film thickness. Such results are unreliable in view of our results in which the film deposited simultaneously on 4 substrates placed side by side had different thicknesses (see Table 5.1). The indirect method of measuring thickness by using a monitor glass slide or rate monitors is very approximate.

5.3 Measurement of Domain Wall Width

The magnetic anisotropy is an important factor in determining the magnetic characteristics of evaporated

films. Films deposited from the vapor phase usually possess a uniaxial component. The films used in this investigation had a small uniaxial anisotropy even though there was no applied field present during the deposition. The direction of the uniaxial anisotropy was not correlated to any specific crystallographic direction and as such the domain pattern did not correspond with the film orientation. Tsukahara and Kawakatsu (1966) also found irregular wall patterns which did not correspond to any definite direction in the lattice. Similar observations have been made by Escudier et al. (1966) and Yelon et al. (1965). The (111) permalloy films grown on (111) Ag of Escudier et al. had an uniaxial anisotropy even though no field was present. They suggest that some stray field might have been present during the evaporation. Yelon et al. on the other hand observed that their (100) films exhibited a small uniaxial anisotropy unrelated to crystallographic axes superimposed on a strong biaxial anisotropy.

For permalloy films near the zero magnetostriction composition and zero crystal anisotropy, magnetic ripple structure is not expected. But the films studied had ripple structure which caused noise in the microphotometer trace. Similar observations have been made in epitaxial permalloy films by Kirenskii et al. (1966b) and Lo (1966). The presence of ripple could be due to nonuniformity of the film as regards to composition. Variations in composition

from place to place in the films could affect the anisotropy through changing amounts of iron-pair ordering and changing magnetostriction.

The images of the walls in the micrographs were not uniformly wide as can be seen from Figures 5.5 through 5.7. The width varied along the length of the wall in every case and the variation is probably due to the presence of ripple structure and variation of anisotropy along the langth of the wall. The wall width was calculated by obtaining a series of micrographs of a wall at different defocussing distances and then measuring the half width of the wall image in each plate at several points along the wall. The half width at zero defocussing distance was obtained by a least squares fit to all the data points. Figure 5.5 shows the image of a wall in a (111) film at four defocussing distances. The calculated half width $w_d(0)$ thus obtained is a measure of the average width of the wall.

In the literature, it is usual to define the asymptotic wall width by

$$w_a \triangleq \frac{\theta_{tot}}{\left[\frac{d\theta(x)}{dx}\right]_{x=0}} \qquad (3.19)$$

where θ_{tot} is the total wall angle. To obtain the half width $w_d(0)$ in terms of w_a, one needs to choose a model for

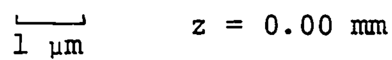

z = 1.85 mm

z = 3.60 mm

z = 6.20 mm

Figure 5.5 Micrographs of a (111) film at different defocussing distances.

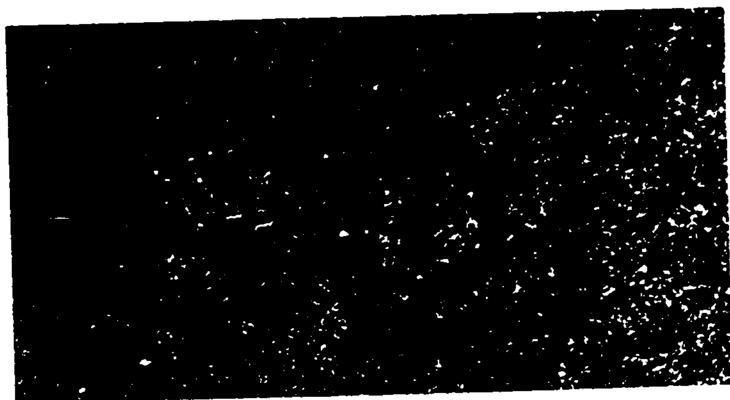

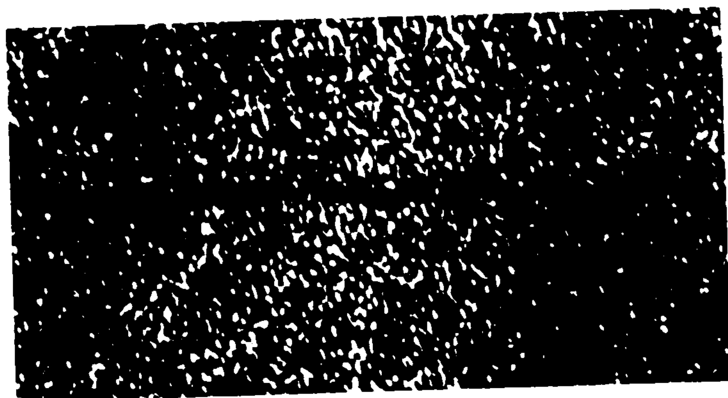

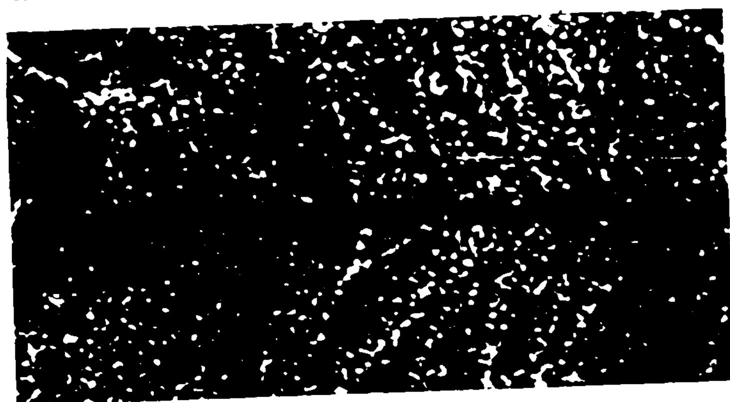

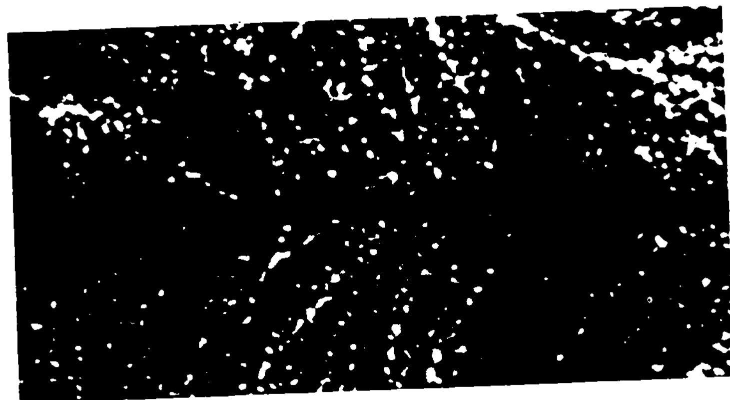

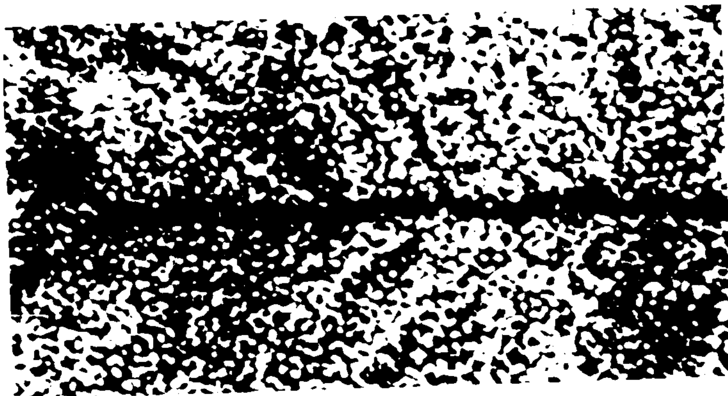

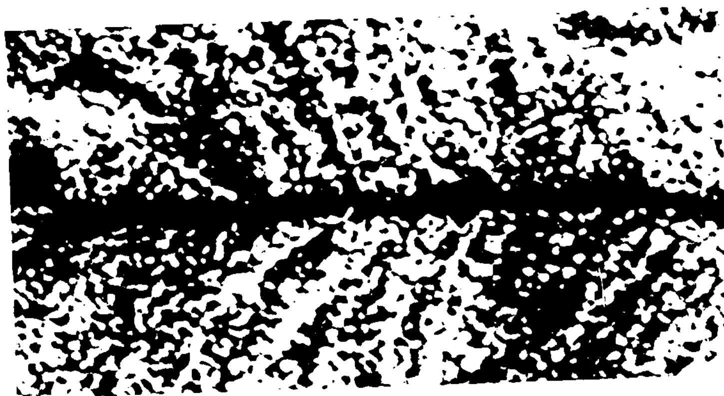

(a)

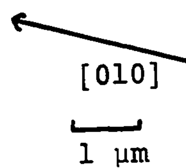

(b)

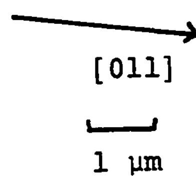

Figure 5.6 (a) 2.374 rad wall in a permalloy film deposited on cleaved (100) NaCl. (b) 1.885 rad wall in a permalloy film deposited on polished (100) NaCl.

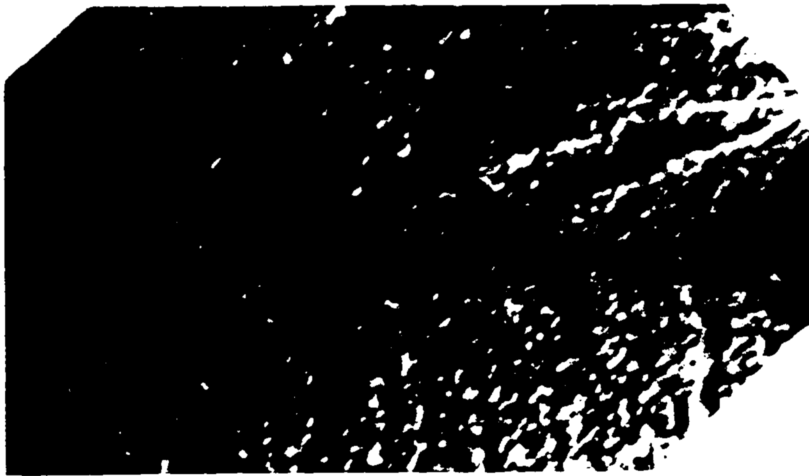

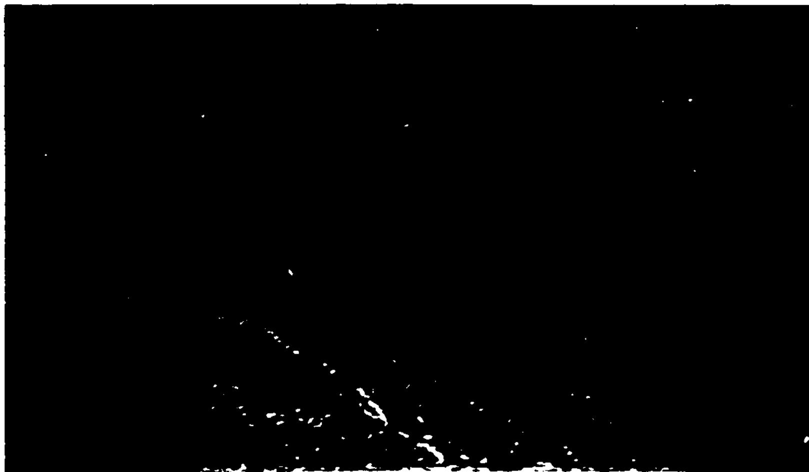

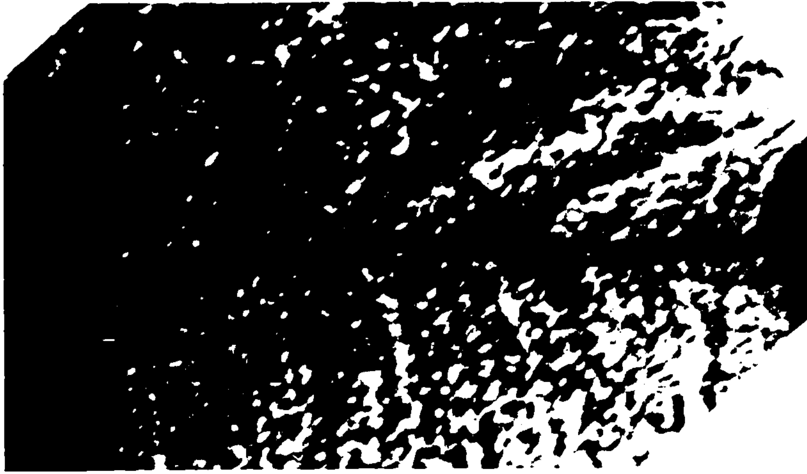

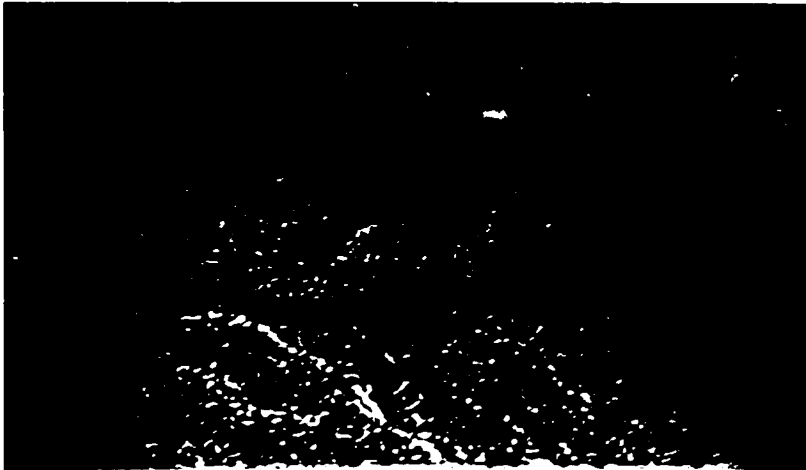

(a)

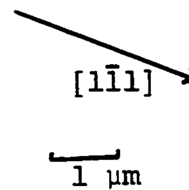

(b)

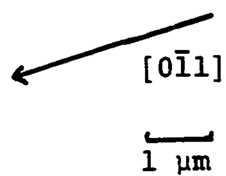

Figure 5.7 (a) 2.217 rad wall in a permalloy film deposited on polished (110) NaCl. (b) 1.990 rad wall in a permalloy film deposited on polished (111) NaCl.

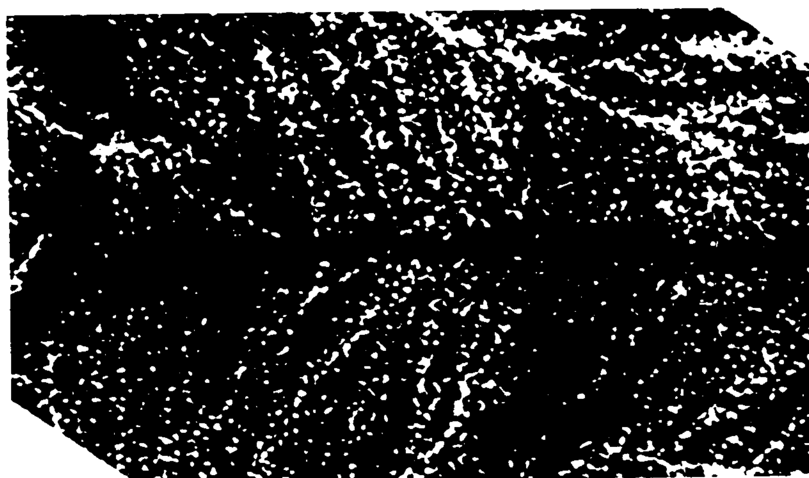

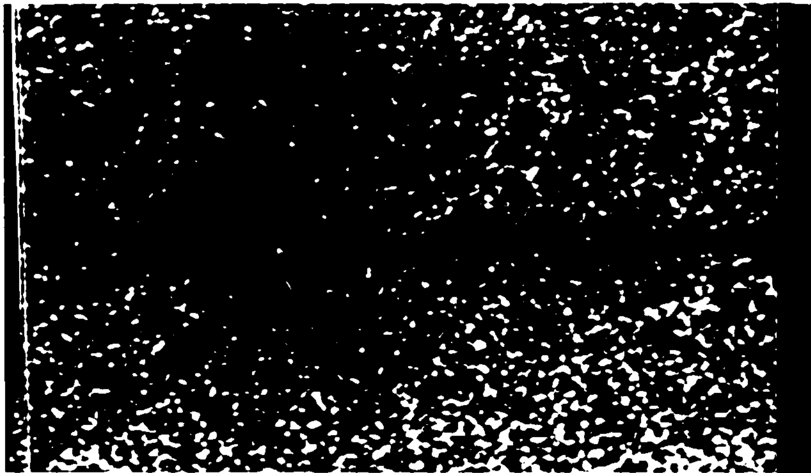

the spin distribution in the wall and we have chosen the Kittel model (see Section 3.5). The relation between the half width $w_d(0)$ and asymptotic wall width w_a is given by

$$w_a = \frac{w_d(0)\ \theta_{tot}}{1.76}. \quad (5.1)$$

For a π radian wall $w_d(0) = 0.56\ w_a$ (Reimer and Kappert 1969a).

All the walls whose widths were measured had θ_{tot} less than π radian. Figures 5.6 and 5.7 show those walls. The values of $w_d(0)$ and w_a are summarized in Table 5.2.

It can be seen that the measured width varies over a wide range as is common in such measurements. No published data on domain wall widths in epitaxial permalloy films is available. Therefore for comparision, the careful measurements made by Cohen and Harte (1969) in polycrystalline films of permalloy (source composition 83% Ni) is given in Table 5.3. It can be seen that the variation is large here also. Part of the reason for such variations may be due to differences in anisotropies of different films.

Film	Thickness (nm)	θ_{tot} (rad)	$w_d(0)$ (nm)	w_a (nm)
(100) cleaved	33	2.374	93.9 ± 13	126.7 ± 18
(100) polished	29	1.885	74.8 ± 12	80.1 ± 13
(110) polished	31	2.217	107.3 ± 11	135.2 ± 14
(111) polished	33	1.990	129.8 ± 15	146.8 ± 17

Table 5.2 Summary of measured wall widths.

Thickness (nm)	θ_{tot} (rad)	w_a (nm)
11.7	2.513	183
25.5	2.112	85
25.5	2.164	64
25.5	2.129	68
25.5	1.920	188
22.5	2.269	313
39.8	1.763	40

Table 5.3 Wall widths in polycrystalline permalloy films measured by Cohen and Harte (1969).

CHAPTER 6

CONCLUSIONS

Epitaxial films of permalloy have been successfully grown under clean evaporation conditions on (100), (110) and (111) faces on NaCl by bombarding the substrates with electrons during the evaporation. The films were well oriented, hole-free and continuous. A comparision of the films produced with and without electron bombardment shows that electron irradiation does indeed play a critical role in the epitaxy of permalloy on NaCl. The density of structural defects in the films was large, but it is consistent with similar observations by other workers in other fcc epitaxial films.

The domain walls studied were not uniformly wide and their width varied from film to film. The wall angles were always less than π radian. Measurement of the width by extrapolating the half widths measured at various defocussing distances is much simpler and more accurate than the method of analysing the variation of intensity across the domain wall width. The measured widths are comparable to those of Cohen and Harte.

Electron microscopic measurement of the magnetic polarization J_s by using the instrument as a small angle diffraction camera is very simple compared to conventional methods of measurement. However the measured values were always less than the bulk values. This is also consistent with the results published in the literature.

There are two major difficulties that are faced by workers in thin films. The first difficulty is that very small amounts of material (10^{-14} m^3) are involved making accurate measurement of magnetic properties difficult. The other difficulty is that of achieveing reproducible results due to the metallurgical 'nightmare' of imperfections, impurities and stress which are always present in evaporated films.

Suggestions for Further Work

To extend the work described in this thesis, wall widths in a number of different permalloy films of different composition and thickness should be measured to obtain a better statistical idea of the dependence of wall width on the various parameters. It might be useful to use a high voltage electron microscope for films thicker than 45 nm.

APPENDIX

DETERMINATION OF HALF WIDTH OF DOMAIN WALLS

The half width $w_d(z)$ of a domain wall as a function of defocussing distance z is given by

$$w_d(z) = 2\, x_{\frac{1}{2}} + 2\, z\, \phi(x_{\frac{1}{2}}) \qquad (3.35)$$

If $w_d(z)$ is plotted as a function z, the intercept of the line given by equation (3.35) on the ordinate gives the half width of the wall at zero defocussing distance, i.e., $w_d(0) = 2\, x_{\frac{1}{2}}$.

About eight pictures were taken of each domain wall at various defocussing distances and the half width of the wall image was measured at 10 to 13 points along the wall on each plate. A straight line was fitted to these 80 to 100 points with the help of a computer by the method of least squares. A typical plot is shown in Figure A.1.

The empirical linear regression lines of the measured half width of the wall image $w_d^i(z)$ on z obtained for the various walls are as follows:

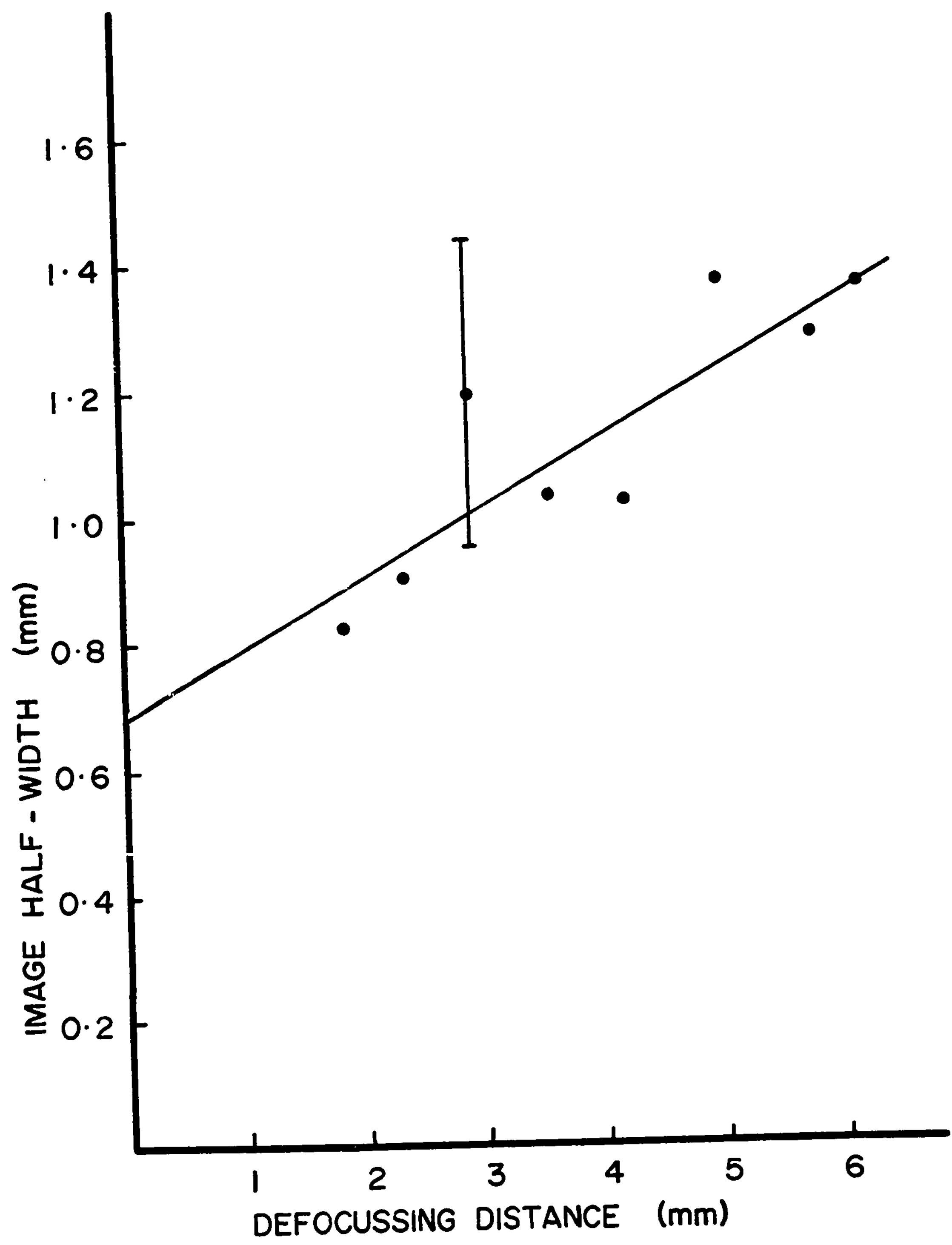

Figure A.1 Plot of the image half width as a function of defocussing distance for 1.990 rad wall in (111) film.

Wall	Regression Line (mm)	(mm) Estimate of Standard Error in $w_d^i(0)$	Image Magnification
100 cleaved	$w_d^i(z)=0.4915+0.1238z$	0.0682	5234
100 polished	$w_d^i(z)=0.4240+0.0994z$	0.0699	5670
110 polished	$w_d^i(z)=0.6161+0.1283z$	0.0630	5741
111 polished	$w_d^i(z)=0.6796+0.1097z$	0.0788	5234

To obtain the actual wall width $w_d(0)$ in the film, the intercept of the ordinate $w_d^i(0)$ is divided by the image magnification.

REFERENCES

Alessandrini, E. I., 1963, J. Appl. Phys., 34, 2518; 1966, Ibid., 37, 4811.

Alpress, J. G., and Sanders, J. V., 1964, Phil. Mag., 10, 827.

Baltz, A., 1963, J. Appl. Phys., 34, 1575.

Bassett, G. A., 1960, in "Proc. European Reg. Conf. Elect. Microscopy," Delft, p. 270.

Bauer, E., Green, A. K., Kunz, K. M., and Poppa, H., 1966, in "Basic Problems in Thin Film Physics" (R. Niedermayer and H. Mayer, eds.), p. 135, Vandenhoeck and Ruprecht, Gottingen.

Behrndt, K. H., 1962, J. Appl. Phys., 33, 193.

Blackburn, W. J. S., Curtis, G. H., and Ferrier, R. P., 1969, J. Scient. Instrum., 2, 570.

Blois, M. S., 1955, J. Appl. Phys., 26. 975.

Boersch, H., and Raith, H., 1959, Naturwissenschaften, 46, 574.

Boersch, H., Raith, H., and Wohlleben, D., 1960, Z. Phys., 159, 388.

Boersch, H., Hamisch, H., Wohlleben, D., and Grohmann, K., 1961a, Z. Phys., 164, 55; 1961b, Ibid., 165, 79; 1962, Ibid., 167, 72.

Boyd, E. L., 1960, IBM J. Res. Dev., 4, 116.

Bozorth, R. M., 1951, "Ferromagnetism." Van Nostrand, Princeton.

Brown, Jr., W. F., 1940, Phys. Rev., 58, 736; 1962, "Magnetostatic Principles in Ferromagnetism." Interscience, New York.

Brown, Jr., and Labonte, A. E., 1965, J. Appl. Phys., 36, 1380.

Burbank, R. D., and Heidenreich, R. D., 1960, Phil. Mag., 5, 373.

Chambers, A., and Prutton, M., 1967a, Thin Solid Films, 1, 235; 1967b, Ibid., 1, 393.

Chambers, A., Lord, D. G., and Prutton, M., 1970, Thin Solid Films, 6, R1.

Chang, H., and Feth. G. C., 1964, IEEE Trans. Comm. Electron., 83, 706.

Chang, H., and Lin, Y. S., 1967, IEEE Trans. Magnetics, Mag-3, 653.

Chikazuki, S., 1961, J. Appl. Phys., 32, 81S.

Chopra, K. L., 1965, Appl. Phys. Letters, 7, 140; 1966, J. Appl. Phys., 37, 2249; 1969, "Thin Film Phenomena." McGraw-Hill, New York.

Chopra, K. L., and Randlett, M. R., 1967, Appl. Phys. Letters, 11, 202.

Cohen, M. S., 1969, in "Thin Film Phenomena" (by K. L. Chopra), p. 608, McGraw-Hill, New York.

Cohen, M. S., and Harte, K. J., 1969, J. Appl. Phys., 40, 3597.

Collins, L. E., and Heavens, O. S., 1957, Proc. Phys. Soc., London, B70, 265.

Craik, D. J., and Griffiths, P. M., 1958, Br. J. Appl. Phys., 9, 279.

Escudier, P., Biragnet, F., Devenyi, J., and Yelon, A., 1966, Phys. Stat. Solidi, 16, 295.

Ferrier, R. P., 1964, in "Third European Regional Conf. on Electron Microscopy," Prague, p. 115.

Ferrier, R. P., and Wade, R. H., 1964, in "Proc. Intern. Conf. Magnetism, Nottingham," p. 873.

Fowler, Jr., C. A., and Fryer, E. M., 1955, Phys. Rev., 100, 746.

Fuller, H. W., and Hale, M. E., 1960a, J. Appl. Phys., 31, 238; 1960b, Ibid., 31, 308S.

Gallon, T. E., Higginbotham, I. G., Prutton, M., and Tokutaka, H., 1968, 2, 369.

Green, A. K., Bauer, E., and Dancy, 1970, J. Appl. Phys., 41, 4376.

Green, A. K., Turner, G., and Bauer, E., 1962, in "Fifth Intern. Congr. Electron Microscopy," Philadelphia, p. GG-6.

Grenga, H. E., Lawless, K. R., and Garmon, L. B., 1971, J. Appl. Phys., 42, 3629.

Grundy, P. J., and Tebble, R. S., 1968, Adv. in Phys., 17, 153.

Hale, M. E., 1958, in "Fifth Symposium of the American Vacuum Society," paper # 41.

Hale M. E., Fuller, H. W., and Rubenstein, H., 1959, J. Appl. Phys., 30, 789.

Hall, C. E., 1966, "Introduction to Electron Microscopy." McGraw-Hill, New York.

Heavens, O. S., 1964, in "Single Crystal Films" (M. H. Francombe and H. Sato, eds.), p. 383, Pergamon Press, New York.

Heavens, O. S., Miller, R. F., Moss, G. L., and Anderson, J. C., 1961, Proc. Phys. Soc., London, 78, 33.

Hemenger, P. M., 1964, Thesis, University of Cincinnati.

Hill, R. M., 1966, Nature, 210, 512.

Hirsch, P. B., Howie, A., Nicholson, R. B., Pashley, D. W., and Whelan, M. J., 1965, "Electron Microscopy of Thin Crystals," Butterworths, London.

Huber, E. E., Smith, D. O., and Goodenough, J. B., 1958, J. Appl. Phys., 29, 294.

Ino, S., 1966, J. Phys. Soc. Japan, 21, 346.

Inuzuka, T., and Ueda, R., 1968, Appl. Phys. Letters, 13, 3.

Jacobs, I. S., 1969, J. Appl. Phys., 40, 917.

Kirenskii, L. V., Sukhanova, R. V., Pyn'ko, V. G., and Edel'man, I. S., 1966a, Bull. Acad. Sci. USSR, Phys. Ser. 30, 53.

Kirenskii, L. V., Sukhanova, R. V., Kan, S. V., Pyn'ko, V. G., and Sivkov, N. I., 1966b, Bull. Acad. Sci. USSR, Phys. Ser. 30, 1373.

Kittel, C., 1949, Rev. Mod. Phys., 21, 541.

Kunz, K. M., Green, A. K., and Bauer, E., 1966, Phys. Stat. Solidi, 18, 441.

Lewis, B., and Jordan, M. R., 1970, Thin Solid Films, 6, 1.

Lo, D. S., 1966, J. Appl. Phys., 37, 3246.

Lord, D. G., 1971, Thin Solid Films, 7, R39.

Mader, S., and Nowick, A. S., 1968, Thin Films, 1, 45.

Mahl, H., and Weitsch, W., 1960, Z. Naturforsch., 15A, 1051.

Matthews, J. W., 1960, in "Proc. European Reg. Conf. Elect. Microscopy," Delft, p. 276; 1965a, Phil. Mag., 12, 1143; 1965b, Appl. Phys. Letters, 7, 131; 1966, J. Vacuum Sci. Tech., 3, 133.

Matthews, J. W., and Allinson, D. L., 1963, Phil. Mag., 8, 1283.

Matthews, J. W., and Grunbaum, E., 1964, Appl. Phys. Letters, 5, 106; 1965, Phil. Mag., 11, 1233.

Middelhoek, S., 1963, J. Appl. Phys., 34, 1054; 1971, in "Magnetic Properties of Materials" (J. Smit, ed.), p. 269, McGraw-Hill, New York.

Néel, L., 1955, Comp. Rend., 241, 533.

Palmberg, P. W., and Rhodin, T. N., 1968, J. Phys. Chem. Solids, 29, 1917.

Palmberg, P. W., Rhodin, T. N., and Todd, C. J., 1967a, Appl. Phys. Letters, 10, 122; 1967, Ibid., 11, 33.

Palmberg, P. W., Todd, C. J., and Rhodin, P. W., 1968, J. Appl. Phys., 39, 4650.

Pascard, H., Hoffmann, F., Sella, C., 1972, Thin Solid Films, 12, 41.

Pashley, D. W., 1959, Phil. Mag., 4, 316; 1965, Adv. in Phys., 14, 327.

Pashley, D. W., and Stowell, M. J., 1962, in "Fifth Intern. Congr. Electron Microscopy," Philadelphia, p. GG-1.

Pashley, D. W., Stowell, M. J., Jacobs, M. H., and Law, T. J., 1964, Phil. Mag., 10, 127.

Poppa, H., 1965, J. Vacuum Sci. Tech., 2, 42.

Ray, S. P., and Paul, D. I., 1970, J. Appl. Phys., 41, 5238.

Reimer, L., and Kappert, H., 1969a, Z. angew. Phys., 26, 58; 1969b, Ibid., 27, 165.

Schoening, F. R. L., and Baltz, A., 1962, J. Appl. Phys., 33, 1442.

Sella, C., and Trillat, J. J., 1964, in "Single Crystal Films" (M. H. Francombe and H. Sato, eds.), p. 201, Pergamon Press, New York.

Shinozaki, S., and Sato, H., 1965, J. Appl. Phys., 36, 2320.

Soohoo, R. F., 1965, "Magnetic Thin Films," Harper and Row, New York.

Stirland, D. J., 1966, Appl. Phys. Letters, 8, 326; 1967/68, Thin Solid Films, 1, 447; 1969, Appl. Phys. Letters, 15, 86.

Suzuki, T., and Wilts, C. H., 1969, J. Appl. Phys., 40, 1216.

Suzuki, T., Wilts, C. H., and Patton, C. E., 1968, J. Appl. Phys., 39, 1983.

Tokutaka, H., and Maejima, R., 1965, J. Phys. Soc. Japan, 20, 362.

Tsukahara, S., and Kawakatsu, H., 1966, J. Phys. Soc. Japan, 21, 313.

Verderber, R. R., and Kostyk, B. M., 1961, J. Appl. Phys., 32, 696.

Wade, R. H., 1962, Proc. Phys. Soc., London, 79, 1237.

Warrington, D. H., 1964, Phil. Mag., 9, 261.

Williams, H. J., and Sherwood, R. C., 1957, J. Appl. Phys., 28, 553.

Williams, H. J., Sherwood, R. C., Foster, F. G., and Kelly, E. M., 1957, J. Appl. Phys., 28. 1181.

Wohlleben, D., 1966, Phys. Letters, 22, 564; 1967, J. Appl. Phys., 38, 3341.

Yelon, A., Voegeli, O., and Pugh, E. W., 1965, J. Appl. Phys., 36, 101.